This document is confidential and is proprietary to the American Chemical Society and its authors. Do not copy or disclose without written permission. If you have received this item in error, notify the sender and delete all copies.

Luminescent Rhenium(I)tricarbonyl complexes containing different pyrazoles and their Successive Deprotonation Products: CO2 Reduction Electrocatalysts

Journal:	*Inorganic Chemistry*
Manuscript ID	ic-2019-03611t
Manuscript Type:	Article
Date Submitted by the Author:	12-Dec-2019
Complete List of Authors:	Merillas, Beatriz; Universidad de Valladolid, Química Inorgánica Cuéllar, Elena; Universidad de Valladolid, Química Inorgánica Díez-Varga, Alberto; Universidad de Valladolid, Química Inorgánica Torroba, Tomas; Universidad de Burgos, Chemistry García-Herbosa, Gabriel; Universidad de Burgos, Química Martín-Alvarez, Jose; Universidad de Valladolid, Quimica Inorganica Miguel, Daniel; Universidad de Valladolid, Quimica Inorganica Villafañe, Fernando; Universidad de Valladolid, Química Inorgánica

SCHOLARONE™
Manuscripts

Submitted to: ***Inorganic Chemistry***

Luminescent Rhenium(I)tricarbonyl complexes containing different pyrazoles and their Successive Deprotonation Products: CO_2 Reduction Electrocatalysts

Beatriz Merillas,[a] Elena Cuéllar,[a] Alberto Diez-Varga,[b] Tomás Torroba,[b] Gabriel García-Herbosa,[b] Jose M. Martín-Alvarez,[a] Daniel Miguel,[a] and Fernando Villafañe[a]

[a] *GIR MIOMeT-IU Cinquima-Química Inorgánica, Facultad de Ciencias, Campus Miguel Delibes, Universidad de Valladolid, 47011 Valladolid, Spain.*

[b] *Departamento de Química, Facultad de Ciencias, Universidad de Burgos, 09001 Burgos, Spain.*

ABSTRACT

Cationic *fac*-[Re(CO)$_3$(pz*H)(pypzH)]OTf (pz*H = pyrazole, pzH; 3,5-dimethylpyrazole, dmpzH; indazole, indzH; 3-(2-pyridyl)pyrazole, pypzH) were obtained from *fac*-[ReBr(CO)$_3$(pypzH)] by halide abstraction with AgOTf and subsequent addition of the corresponding pyrazole. Successive deprotonation with Na_2CO_3 and NaOH gave the neutral *fac*-[Re(CO)$_3$(pz*H)(pypz)] and anionic Na{*fac*-[Re(CO)$_3$(pz*)(pypz)]} complexes, respectively. The cationic, neutral complexes and *fac*-[Re(CO)$_3$(pypz)$_2$Na] were subjected to photophysical and electrochemical studies. They exhibit phosphorescent decays from a prevalently ^{3}MLCT excited state with quantum yields (Φ) in the range between 0.03 and 0.58, and long lifetimes (τ from 220 to 869 ns). The electrochemical behavior in Ar atmosphere of

cationic and neutral complexes indicates that the oxidation processes assigned to $Re^{I} \rightarrow Re^{II}$ occurs at lower potentials for the neutral compared to cationic complexes. The reduction processes occur at the ligands and do not depend on the charge of the complexes. The electrochemical behavior in CO_2 media is consistent with CO_2 electrocatalyzed reduction, where the values of the catalytic activity [$i_{cat}(CO_2)/i_{cat}(Ar)$] ranged from 2.7 to 11.5 (compared to 8.1 for *fac*-[$Re(CO)_3Cl(bipy)$] studied as a reference). These values are higher for indazole complexes and may be related to the acidity of the coordinated pyrazole.

INTRODUCTION

The first report on the photophysical properties of rhenium(I) tricarbonyl diimine complexes was described 45 years ago.[1] Since then, this class of compounds has been very intensively studied, and many luminescent *fac*-[$ReX(CO)_3(N\text{-}N)$] complexes have been reported, showing rich excited-state properties associated with their long-lived triplet metal-to-ligand charge transfer (^{3}MLCT) excited state.[2] The study of these photophysical properties has led to the development of diverse applications for this type of compounds, such as biomolecular agents,[3] molecular sensors or photoswitches,[4] light-emitting devices,[5] photocatalysts for the reduction of CO_2,[6] or for the production of H_2.[7]

These applications are usually the result of an adequate tuning by varying the diimine ligand, the "sixth" ligand "X" (a halide or pseudo halide for neutral complexes, a neutral ligand for cationic complexes), or the solvent.[2] An alternative and efficient strategy in order to induce systematic and tunable modifications in the donor/aceptor properties of the ligands emerges from the presence of either acidic hydrogens or protonatable sites. They allow reversible protonation/deprotonation processes in mild conditions, thus favoring smooth differences in the electron distributions of the ground and the excited states, and therefore

helping to adjust their photophysical properties.[6c,8] However, there are scarce reports on the role of ligands able to undergo protonation/deprotonation processes on the chemical and physical properties of rhenium(I) tricarbonyl diimine complexes. The first report described the absorption and luminescent properties of several complexes containing carboxylic acid-functionalized ligands.[9] The use of diimine ligands bearing acidic phenol substituents,[10] or imidazole groups,[11] as well as reports on oxazolylidene or tetrazolate moieties as "sixth" ligand[12] have also been described. There are also reports on the involvement of ligands with acidic hydrogens or protonatable sites in proton-coupled electron transfer (PCET) processes on photoexcited rhenium(I) tricarbonyl diimine complexes.[13]

Following our aim to design systems which allow a systematic control of both the electronic and steric properties of the ligands coordinated to the *fac*-[$Re^{I}(CO)_3$)] fragment,[14] we devised a family of complexes destinated to allow successive deprotonations in order to obtain cationic, neutral and anionic compounds with similar ligands but different electronic and steric properties. Herein we report the syntheses, photophysical, and electrochemical properties of cationic *fac*-[$Re(CO)_3$(pz*H)(pypzH)]OTf (Scheme 1; pypzH = 2-pyridyl-3-pyrazole; pz*H = pyrazole, pzH; 3,5-dimethylpyrazole, dmpzH; indazole, indzH; or pypzH), and of the complexes obtained after their sucessive deprotonations: neutral *fac*-[$Re(CO)_3$(pz*H)(pypz)] and anionic Na[*fac*-$Re(CO)_3$(pz*)(pypz)] (Scheme 1). Their luminescence and their electrochemistry is herein described and compared to those of other complexes closely related which have been previously reported, such as the parent complex which contains a bromido and pypzH,[15] or those containing bipy as diimine ligand and other pyrazolates as "sixth" ligand.[16]

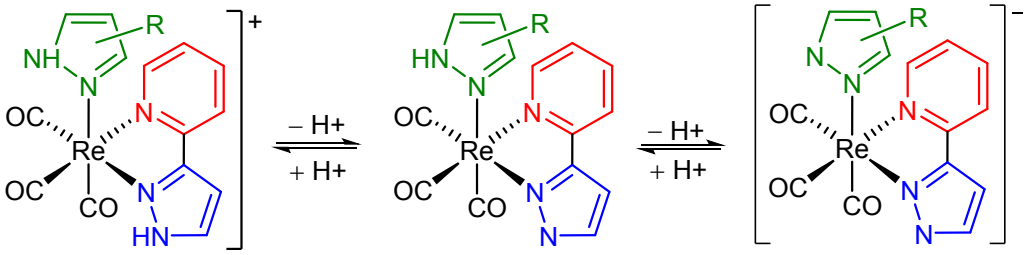

Scheme 1. Compounds herein described (pz*H = pzH, dmpzH, indzH, pypzH).

As indicated above, one of the more attractive applications of this type of complexes is their role as catalysts for photochemical CO_2 reduction, since it is related with probably the most important issue worldwide today, such as global warming and the shortage of fossil-fuel resources.[6] Nowadays, it is widely accepted that the incorporation of a proton source in the substrate facilitates the catalytic process via intramolecular hydrogen bonding interactions, that may eventually alter the reaction products, and therefore allow to tune the selectivity of the reaction. Although the concept of local proton source was firstly applied in iron porphyrins,[17] several recent reports describe reductions of CO_2 catalyzed by rhenium(I) tricarbonyl diimine complexes with ligands containing different proton sources.[18] This led us to explore the catalytic activity towards CO_2 reduction of the complexes herein described.

DISCUSSION AND RESULTS

Syntheses and characterization of the complexes

The reaction of *fac*-[ReBr(CO)$_3$(pypzH)] (**1**)[19] with a slight excess of AgOTf (OTf = O_3SCF_3) leads to the precipitation of AgBr and to *fac*-[Re(OTf)(CO)$_3$(pypzH)] (**2**), which results from the substitution of the bromido ligand by the more labile triflato (Scheme 2). The reaction occurs in THF, so the presence in solution of *fac*-[Re(THF)(CO)$_3$(pypzH)](OTf) can not be discarded (see Experimental). The triflato (or THF) ligand is then substituted by different

pyrazoles (pzH, dmpzH, indzH, or pypzH), so cationic pyrazole complexes *fac*-[Re(CO)$_3$(pz*H)(pypzH)]OTf (**3**) (pz*H = pzH, **3a**; dmpzH, **3b**; indzH, **3c**; pypzH, **3d**) are obtained after 24 h at 40 ºC.

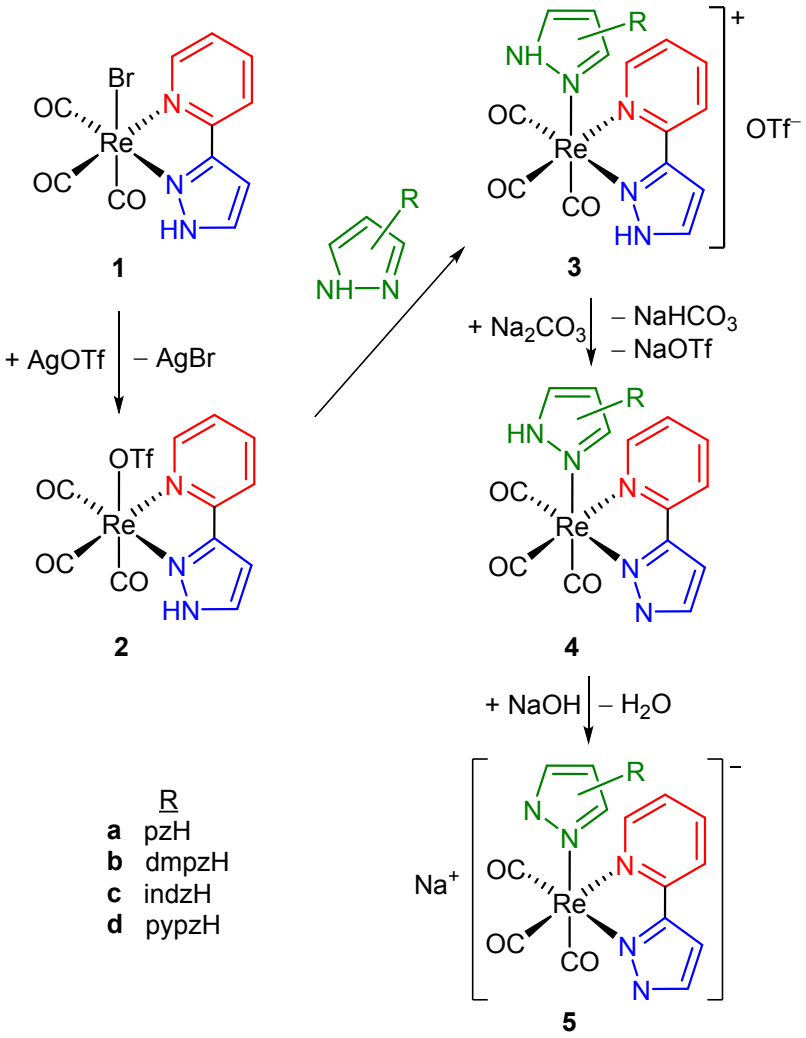

Scheme 2: Syntheses of the complexes.

The NH protons of the pyrazole and of the pypzH ligands are acidic, so as one of them can be easily removed by treatment with Na_2CO_3. These reactions afford the neutral complexes *fac*-[Re(CO)$_3$(pz*H)(pypz)] (**4**) (pz*H = pzH, **4a**; dmpzH, **4b**; indzH, **4c**; pypzH, **4d**; Scheme 2). The proposal of a deprotonated pypz and a protonated pyrazole in complexes **4a-d** is based in the crystal structure of **4a** (see below). However in solution this proton might

be delocalized among both nitrogen donor atoms of the pyrazolate and pypz groups, as discussed below.

Deprotonation of the remaining proton requires a stronger base, and the anionic complexes Na[*fac*-Re(CO)$_3$(pz*)(pypz)] (**5**) (pz* = pz, **5a**; dmpz, **5b**; indz, **5c**; pypz, **5d**; Scheme 2) are obtained in solution after reaction of **4a-d** with the equimolar amount of aqueous NaOH. Complex **5d** had been previously synthesized by an alternative method, and was then completely characterized.[19] All the attempts to isolate the rest of anionic complexes **5a-c** were unsuccessful, due to their high instability both in the solid state and in solution. The presence of an extra nitrogen donor atom in **5d** (Figure 1) might explain the higher stability of this complex. In fact, similar manganese(I) complexes of formula [{*fac*-Mn(CO)$_3$(μ^2-pypz)(μ-pypz)M}$_n$] (M = Li, n =1; M = Na, K; n =2) could be also crystallographically characterized.[19] Therefore, complexes **5a-c** are herein characterized by ^{1}H NMR and IR in solution after deprotonation of the corresponding cationic or neutral complexes **3a-c** or **4a-c** (see Experimental).

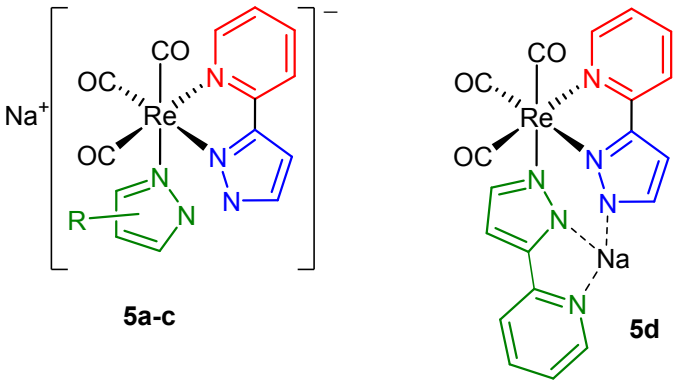

Figure 1. Complexes Na[*fac*-Re(CO)$_3$(pz*)(pypz)] (pz* = pz, **5a**; dmpz, **5b**; indz, **5c**; pypz, **5d**).

Complexes **3a**, **3d**, and **4a** have been characterized crystallographically. The crystal structures are displayed in Figure 2, and distances and angles may be obtained from the cif (see Supplementary Information). As expected, rhenium shows an octahedral coordination in all the structures, and the distances and angles are similar to those found in the crystal structures of other pypzR rhenium(I) tricarbonyl complexes.[20] The acidic proton of the pyrazolyl unit in the neutral complex **4a** was localized in the pyrazole, and it is involved in hydrogen bonding with the deprotonated nitrogen of the pypz moiety (Figure 2, below, right). In the structures of the cationic complexes **3a** and **3d**, the N-bound hydrogens of the pyrazoles or pypzH ligands are also involved in hydrogen bonding with molecules of solvent present in the crystals or with the anion. The distances N-H···E (E = heteroatom), N ···E, and the angles N-H···E are in accordance with "weak" or "moderate" hydrogen bonds.[21]

The spectroscopic and analytical data are included in the Experimental Section and support the proposed geometries. The only acidic proton present in the neutral complexes **4a-d** is very probably involved in a fast exchange equilibrium between both basic nitrogen atoms in both pyrazolyl groups, as it could only be detected as a broad signal in the ^{1}H NMR of dmpzH complex **4b** (see Experimental), whereas it is too broad to be detected for the rest of neutral complexes. This fact might be related with the higher basicity of dmpz compared to the rest of pyrazolates herein employed,[22] what might explain the larger energetic difference between the dmpzH-pypz and dmpz-pypzH tautomers compared to those where the rest of pyrazolyl groups are involved.

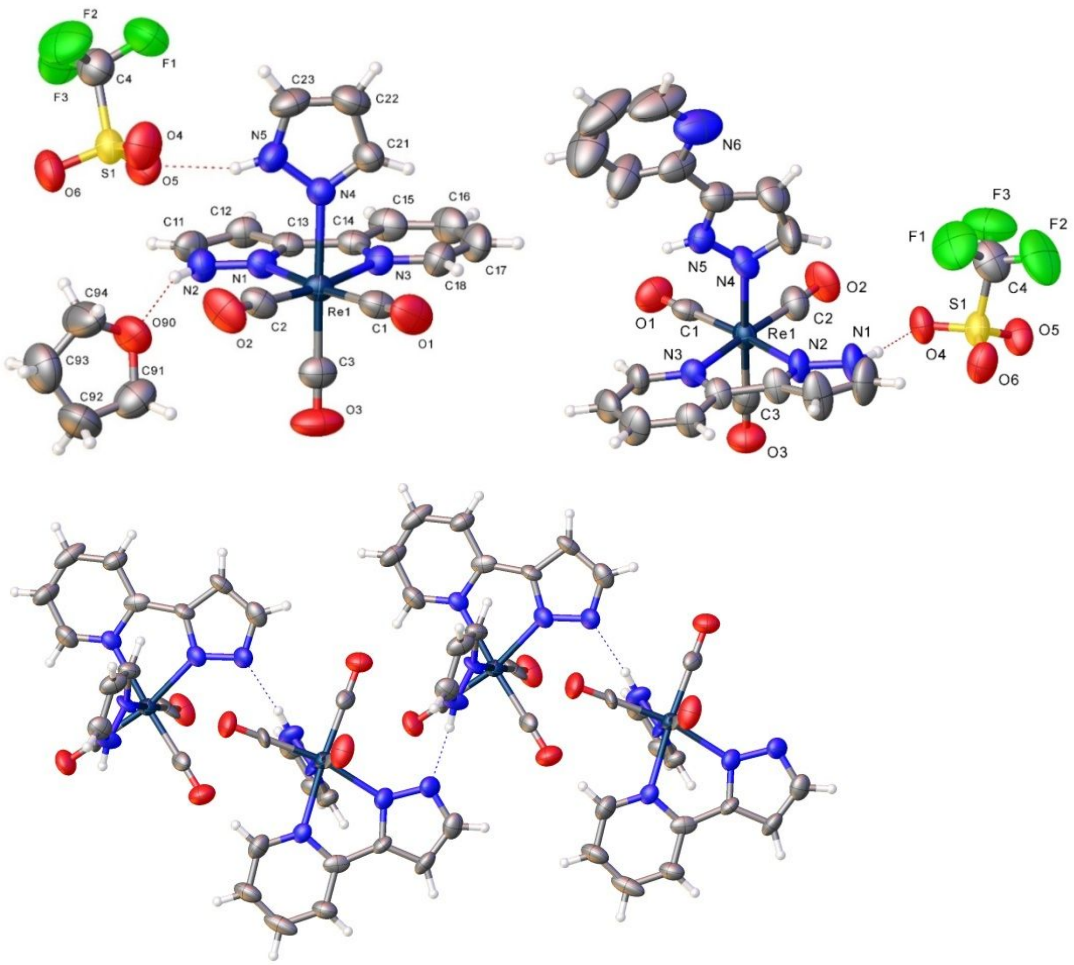

Figure 2. Perspective views of **3a** (above, left), **3d** (above, right), and **4a** (below). Thermal ellipsoids are drawn at 30% probability.

The protonation/deprotonation equilibria among the cationic (**3a-d**), neutral (**4a-d**) and anionic (**5a-d**) species revealed to be fast, since mixtures of them give always averaged spectra. The variation of the chemical shifts for mixtures containing different species was determined as a function of the amount of hydroxide anion added to a solution of **3b**, what allowed to obtain successively **4b** and **5b** (Figure S1).

Photophysical studies

The main absorption and emission spectral data for complexes **3a-d**, **4a-d**, and **5d** are summarized in Table 1. The absorption and emission spectra, as well as the wavelengths

detected in different solvents at 298 K are collected in Figure S2. All the complexes display intense absorption bands in the 250-300 nm region which may be attributed to π(L)→π*(L) IL, and low energy broad bands in the near UV region, above 300 nm, corresponding to dπ(Re)→π*(L) MLCT. The different nature of the absorptions is confirmed by the solvatochromic nature of the MLCT absorptions, where larger electric dipole changes are associated with the electronic transitions. Thus, 15 nm to even 60 nm blue shifts are observed in the MLCT bands when going from less polar $CHCl_3$ to more polar MeCN (Figure S2). Meanwhile, the transitions assigned to IL π-π* are associated with minimal electric dipole changes and therefore are almost insensitive to the solvent change. These assignments are based on the absorption spectra of closely related metal complexes, which display similar bands, such as 271 and 352 nm for **1** in $CHCl_3$.[15] The similar high-energy MLCT transitions displayed by **1** and **3a-d** or **4a-d** (ca. 355 nm, see Table 1) indicates that the replacement of bromido ligand in **1** by different pyrazoles (complexes **3a-d**) does not seem to affect the dπ(Re) orbital energy. On the other hand, no significative variations are observed when comparing the absorption spectra maxima of each neutral with the corresponding cationic complex (each complexes **3a-d** *vs*. each **4a-d**), as previously reported for the deprotonation of a Re(I) complex containing 2-(2'-pyridyl)benzimidazole as chelating ligand.[11] This contrasts with the deprotonation of **4d** to afford **5d**, which occurs with a hypsochromic shift (*ca*. 40 nm), as previously described for the deprotonation of different $Re^{I}(CO)_3$ complexes containing 5-aryl tetrazoles, coordinated as "sixth" ligand.[12b]

Table 1. Absorption and emission data of complexes in $CHCl_3$.

Comp	Absorption	Emission				
	λ nm (ε x 10^{-3} $M^{-1}cm^{-1}$)	λ_{em} nm [λ_{excit} = 360 nm]	**Ø** x 10^{-2} (± 8%)	**τ** (ns)	$\mathbf{k_r}$ 10^5 s^{-1}	$\mathbf{k_{nr}}$ 10^5 s^{-1}
1[15]	271 (25.0), 352 (2.5)	519	5.0	188	26.5	504.9
3a	267 sh (12.1), 290 (8.7), 335 (3.2)	497	43	392	11.0	14.5
3b	252 sh (8.2), 297 (2.8), 366 (0.2)	497	3,1	341	0.9	28.4
3c	268 (21.8), 287 sh (15.9), 300 sh (11.9), 352 (2.8)	494	21	490	4.3	16.1
3d	266 sh (18.6), 283 (19.4), 360 (2.3)	499	58	610	9.5	6.9
4a	256 (13.1), 296 (8.0), 324 (4.9), 355 sh (2.8)	504	17	696	2.4	11.9
4b	259 (10.4), 273 sh (8.8), 298 (5.2), 359 (1.9)	502	11	281	3.9	31.7
4c	269 (20.8), 289 sh (14.6), 299 sh (10.8), 364 sh (1.3)	495	23	869	2.6	8.9
4d	276 (20.1), 295 sh (17.7), 318 sh (11.1), 350 sh (4.1)	501	31	591	5.2	11.7
5d	236 (7.2), 313 (6.9)	508	2.6	220	1.2	44.5

Some of the complexes were also studied theoretically by means of density functional and time-dependent density functional theory (TD-DFT) calculations. Computational details can be found in the Experimental section, and the complete list of results are included in the Supplementary Information. The ground-state geometries were optimized at the PBE1PBE level (PBE0) with no symmetry restraints for the complexes studied and the minimum obtained compares well with both crystal structures obtained by X-ray diffraction. As shown in Figure 3, the calculations results are consistent with the band shapes of the optical spectra of **3c**. In order to compare analogous cationic and neutral complexes, frontier Molecular Orbital calculations in the ground state at the PBE1PBE level for complexes **3a** and **4a** (Tables S1 and S2) confirms that the HOMO-LUMO energy gap is very similar for both complexes (3.800 eV for **3a** *vs*. 3.998 eV for **4a**). However, the relative contribution of the orbitals differs: the HOMO of **3a** has a mixed **Re**/**CO**/**pzH** (58.3/23.4/13.8) character, whereas that of **4a** has a mixed **Re**/**CO**/py**pzH** (38.7/19.0/38.1) character. The LUMOs are localized almost exclusively on the pypz fragment, with higher contribution from the pyridine ring, specially in neutral **4a** (py/pz = 58.4/32.9 for **3a**, py/pz = 76.0/14.8 for **4a**). We have

been able to find only one precedent of such a different contribution between both rings of a diimine ligand, specifically in pyridyltriazolato ligands.[23]

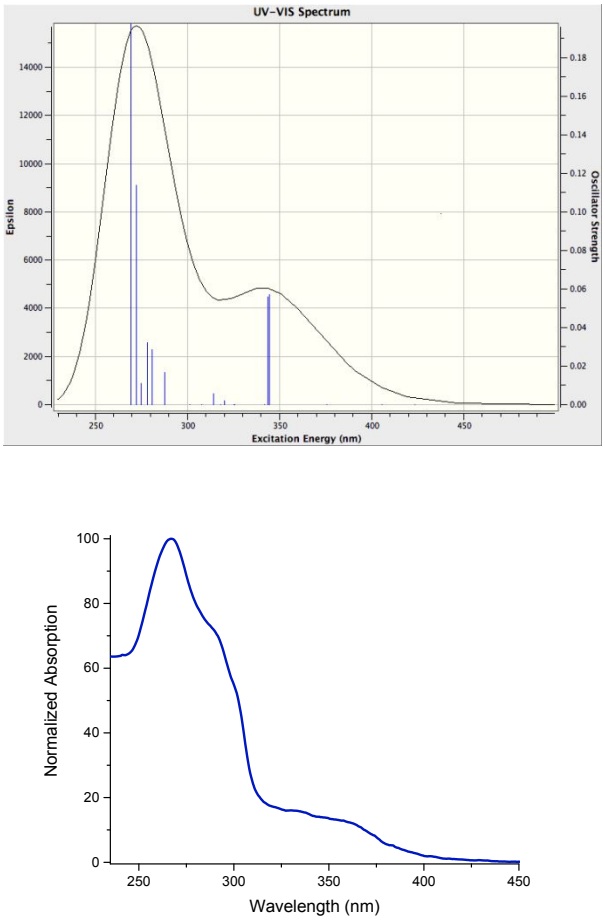

Figure 3. Calculated (above) and experimental (below) absorption spectra for **3c**.

The emission spectra of all the complexes show one unstructured broad band, which is solvent-dependent (3-16 nm shifts for **3a-d**, 14-41 nm shifts for **4a-d**, 33 nm shift for **5d**). The intensities in the emission spectra of all the complexes show a dramatic increase in deaerated solutions compared to those prepared without exclusion of air, with no variation in the emission maxima (see Figure S2 in Supplementary Information). These results, along with luminiscent emission lifetimes (see below), are characteristic features of ^{3}MLCT phosphorescent emissions.[2] Deprotonation of complexes **3a-d** to afford the corresponding **4a-**

d and futher deprotonation of **4d** to ontain the anionic **5d** takes place with a slight bathochromic shift of the emission band (1-7 nm). This contrasts with previous reports of deprotonation of different NH groups present in the ligands, where blue-shifts (48 nm) are detected when deprotonation occurs in the diimine ligands,[11] whereas deprotonation in the "sixth" ligand induced red-shift (50-58 nm) of the emission bands.[12]

The quantum yields of **3a-d**, **4a-d**, and **5d** are similar to those previuosly reported for other rhenium(I) tricarbonyl complexes containing azolates as "sixth" ligands,[16,24] or azolyl fragments in the diimine ligand.[15,20b,23,25] The comparison among the quantum yields of cationic complexes **3a-d** with those of their corresponding deprotonated neutral complexes **4a-d** and also with that of the anionic **5d** leads to significative variations for the pz (0.43 for **3a** vs. 0.17 for **4a**) and pypz (0.59 for **3d**, 0.31 for **4d** and 0.026 for **5d**) complexes. Similar decreases were observed for similar deprotonations occurred in complexes containing NH groups in either the "sixth"[26] or in the diimine ligands.[11,12b]

Finally, the luminescent emission lifetimes are in the range of those previously reported for similar Re complexes.[16,23,24,25a,25d] No relevant variations are observed depending of whether the complex is cationic, neutral or anionic, as previously reported for similar systems able to undergo acid-base processes.[11,12b,26]

Electrochemical studies

The cyclic voltammetries of complexes **1**, **3a-d**, **4a-d**, and **5d** show an electrochemical behavior consistent with CO_2 activation, i.e. electrocatalyzed reduction (see Figures S3 to S18 in the Supplementary Information). As a representative example, the results registered for complex **3c** are shown in Figure 4. Blue (corresponding to the experiment performed in CO_2 atmosphere) and red (experiment performed in Ar atmosphere) traces overlap completely in the range −1.5 V to +2.0 V. The black trace corresponds to the window of the blank, i.e. the

solvent plus the supporting electrolyte. Changing the atmosphere from Ar to CO_2 a great enhancement of the current at potentials below –2.0 V is observed.

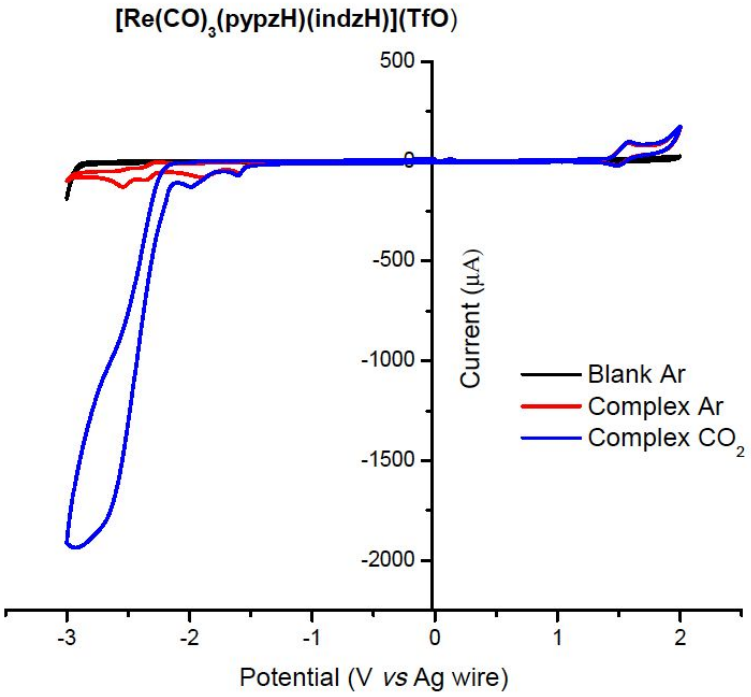

Figure 4. Cyclic voltammograms of *fac*-[Re(CO)$_3$(pypzH)(indzH](TfO) (**3c**) under Ar (red trace) and under CO_2 (blue trace). See SI and experimental sections for details.

Table 2 gathers the observed potential values referenced to the redox pair ferrocenium/ferrocene, following the IUPAC recommendations.[27] The experimental raw values observed using silver wire (as pseudoreference electrode) or AgCl/Ag (3M NaCl reference electrode) are collected in Tables S3 and S4. The ratio $\frac{i_{cat}(CO_2)}{i_{cat}(Ar)}$ ranges from 2.7 to 11.5 and allows to compare the catalytic activity of the complexes.

Neutral complexes **1** and **4a-d** (under Ar) have a common pattern in the anodic scan to positive potentials that consists of one irreversible peak in the range 0.61-0.96 V, followed by a second reversible wave in the range 1.08-1.36 V. A similar behavior has been previously reported for analogous [ReX(CO)$_3$(diimine)] (X = Cl, Br) complexes, as well as a mechanistic

proposal.[28] The oxidation of cationic complexes **3a-d** occurs, as expected by simple coulombic considerations, to more positive potentials.

Table 2. Electrochemical data obtained by cyclic voltammetry in this study and referenced to the redox system ferrocenium/ferrocene.[a]

Complex	Observed E_{pk}^{ox} and E_{pk}^{red} values[b]		$i_{cat}(Ar)$[c]	$i_{cat}(CO_2)$[c]	Ratio[d] $i_{cat}(Ar)/i_{cat}(CO_2)$
	Anodic scan	Cathodic scan			
fac-[ReCl(CO)$_3$(bipy)]		–1.78 –2.15	–24	–195	8.1
1	0.41[e], 0.96, 1.36[r]	–2.04, –2,14	–133	–953	7.2
3a	1.21[r]	–1.94, –2.30, –2.74, –2.89	–200	–1300	6.5
3b	1.19[r]	–1.15, –2.30, –2.75	–166	–1400	8.4
3c	1.26[r]	–1.87, –2.18, –2.64, –2.81	–168	–1935	11.5
3d	1.12[sh], 1.29	–2.10, –2.65	–94	–800	8.5
4a	0.70, 1.19[r]	–2.63, –2.93	–57	–490	8.6
4b	0.67, 1.10[r]	–2.40, –2.74, –2.98	–114	–303	2.7
4c	0,74, 1.26[r]	–2.20, –2.64	–52	–590	11.3
4d	0.39, 0.61, 1.08[r]	–2.72	–58	–562	9.7
5d	0.34, 0.54, 0.96[r]	–2.77	–55	–311	5.6

(a) The reduction potential mean value observed for Ferrocenium/Ferrocene (Fc^+/Fc) used as internal calibrant under the employed experimental conditions was E^0 = 0.443± 0.005 V *vs*. the AgCl/Ag (3M NaCl) electrode (see values at Table S4).
(b) Anodic or cathodic scan peaks observed under Ar unless stated otherwise.
(c) Maximum registered cathodic current (μA) under Ar, $i_{cat}(Ar)$, or under CO_2, $i_{cat}(CO_2)$.
(d) Ratio between the Faradaic currents observed under Ar, $i_{cat}(Ar)$, or under CO_2, $i_{cat}(CO_2)$.
(e) Assigned to bromide earlier for the analogous *fac*-[MnBr(CO)$_3$(pypzH)].[19] This peak appears in the reverse of the cyclic scan from 0V to +2V to 0V (See Figure S4).
(r) Waves where both peaks i_{ox} and i_{red} were observed. Value of $E_{1/2}$ is given in those cases.
(sh) Shoulder, not resolved peak (see Figure S13).

The values of the peak potentials observed at cathodic scans (under Ar) seem quite erratic. The change of bromido-pyridylpyrazole (neutral complex **1**) by pyrazole-pyridylpyrazolate (neutral complexes **4a-d**) renders reduction more difficult (more negative potential values observed). For cationic pyrazole-pyridylpyrazole complexes **3a-d**, the potentials shift to less negative values, i.e. adding electrons becomes easier, as expected when the charge of the complexes changes from zero to +1. Two, three or even four peaks are observed depending on the complex. Previous mechanistic studies indicate that several different species might account for the observed peaks at cathodic scans.[6a] Furthermore,

deprotonation in complexes **3a-d** may add new active species, as reported previously for similar imidazole complexes.[29] In spite of the random cathodic scans under argon, a parallel behavior is observed under CO_2 which consists in a large enhancement of the cathodic current associated to the reduction of CO_2 (see Figure 4 and Figures S3 to S18 in the Supplementary Information).

The electrocatalytic reduction of CO_2 by *fac*-[ReCl(CO)$_3$(bipy)] has been recognized and explored since the report by Lehn *et al*. in 1984.[30] It is very difficult indeed to compare the catalytic activity on the basis of overpotentials and current enhancement values reported. Such data are strongly dependent both on the working electrode and on the solvent used. Also, dryness of the solvent is crucial. Therefore, for comparison purposes we have repeated electrochemical measurements of *fac*-[ReCl(CO)$_3$(bipy)] under the same experimental conditions than for the complexes herein reported. The cyclic voltammograms of *fac*-[ReCl(CO)$_3$(bipy)] are depicted in Figure S3, and potentials collected in Table 2. The enhancement ratio of the cathodic currents is $\frac{i_{cat}(CO_2)}{i_{cat}(Ar)} = 8.1$ and the maximum of the cathodic current was observed at –2.86 V (*vs.* Fc^+/Fc).

We have previously reported the electrochemistry of **1** under N_2 at a platinum electrode using the SCE reference electrode in THF.[19] Herein we report the electrochemistry at a GC (glassy carbon) electrode in dry MeCN using the AgCl/Ag reference electrode. The different working electrodes and solvents used led to important differences, what supports the feasibility to make comparisons only when the experimental conditions are exactly the same. Under Pt/THF only one single-electron irreversible oxidation wave assigned to $Re^I \rightarrow Re^{II}$ at E_{pk}^{ox} = 1.615 V *vs*. SCE (1.070 V *vs*. Fc^+/Fc) was detected.[19] Under GC/MeCN we now observe (Figure S4 and Table S4) the one-electron irreversible oxidation at E_{pk}^{ox} = 1.40 V *vs*. AgCl/Ag (NaCl, 3M) (0.96 V *vs*. Fc^+/Fc), followed by an apparently reversible wave at $E_{1/2}$= 1.80 V *vs*. AgCl/Ag (NaCl, 3M). Comparable anodic scan pattern and potentials have been reported for

complexes fac-[ReX(CO)$_3$(bipy)] (X = Cl, Br), including detailed mechanistic insights which may be applied to our complexes.[28] Related complexes with different aromatic diimines generally show irreversible oxidation waves between 0.9 and 1.2 V *vs*. Fc^+/Fc.[31] The Re^I/Re^{II} couple was reported to be "quasi-reversible" for a six-membered chelate ring diimine.[32] The small peak (more prominent under CO_2) at +0.85 V (*vs*. AgCl/Ag) that was reported for *fac*-[MnBr(CO)$_3$(pypzH)] under Pt/THF but not for **1** under Pt/THF,[19] is here assigned again to the presence of bromide ion. The role of bromine during the oxidation of related rhenium(I) tricarbonyl diimine complexes has been already reported.[28,33]

The electrochemistry of **1** scanning to negative reduction potentials (cathodic scan) had not been reported to date. On the basis of the electrocatalytic activity of *fac*-[ReCl(CO)$_3$(bipy)] for the reduction of CO_2 and its structural and electronic similarity with **1**, we decided to explore its electrochemical behavior both under argon and under carbon dioxide, what led to observe a 5-fold current enhancement at –2 V (see Figure S4) for the latter. This experiment points to the need for scanning to more negative potentials (< –2 V). Therefore, cyclic voltammograms of **1** were recorded in the range +1 V to –3 V (see Figure S5). In order to avoid adventitious undesired water from the AgCl/Ag (3M NaCl) reference electrode, a silver wire was used as pseudo-reference electrode, and ferrocene was added at the end of the measurements as internal calibrant. As displayed in Figure S5 (red trace), scanning to negative potentials under Ar led to several waves indicating that the complex undergoes successive electron transfer reductions. Repeating the same scan under CO_2 leads to intense enhancement of the cathodic current. The maximum cathodic current under CO_2 was found at –2.78 V (*vs.* Fc^+/Fc). At this potential, the ratio of the cathodic current is $\frac{i_{cat}(CO_2)}{i_{cat}(Ar)} = 7.2$. According to these experimental results, the electrocatalytic activity of complexes *fac*-[ReCl(CO)$_3$(bipy)] and **1** are quite similar. The different shapes of the waves associated to electrocatalytic reduction of CO_2 come from the competition at the electrode surface between

CO_2 consumption (related to the rate-determinant step of the catalytic cycle) and the arrival of new substrate by diffusion.[6c]

Neutral complexes **4a-d** formally result from the substitution of the bromido anionic ligand in complex **1** by different pyrazolates, even though the remaining acidic proton is formally bonded to the pyrazole, as discussed above. In all the complexes the first oxidation peak (related to the HOMO) is shifted to less positive potentials, indicating that the couple pyridylpyrazolate-pyrazole is better donor than the pyridylpyrazole-bromido pair. This is confirmed by the IR ν_{CO} wavenumbers (ν_{CO} average 1944.7-1946.7 cm^{-1} for **4a-d** *vs*. 1950.7 for **1**,[19] in THF).

The complex **4a** is poorly soluble in MeCN, in fact it was measured as a cloudy mixture, instead of a clear solution. The observed anodic scan pattern (see Figure S14) reproduces that observed for **1** but shifted to lower potentials (see Table 2), as pointed out in the precedent paragraph. A small peak sometimes detected on oxidative scans, at ca. +0.2 V, may be attributed to coatings of the working electrode formed when very negative potentials have been previously reached, being cleaned in the following scan to positive potentials. Note in Table 2 that more negative potentials are needed to reduce **4a** compared to **1**, what would indicate that pyrazolate ligand destabilizes the LUMO. The cathodic current enhancement is $\frac{i_{cat}(CO_2)}{i_{cat}(Ar)} = 8.6$.

Under anodic scan to positive potentials, **4b** repeats the same pattern (Figure S15) as the analogous unmethylated **4a**. However, the observed potentials shift to more positive values under CO_2 atmosphere (green trace in Figure S15), suggesting that CO_2 modifies the chemical steps that follow the first electron transfer. The maximum cathodic current under CO_2 is found at –3.09 V (*vs*. Fc^+/Fc), and the ratio of the cathodic currents is $\frac{i_{cat}(CO_2)}{i_{cat}(Ar)} = 2.7$, the lowest for all the complexes herein described.

Complex **4c** is poorly soluble in MeCN, leading to a cloudy mixture in the electrochemical cell. The anodic scan reproduces previous patterns (see Figure S16). No shifts are observed when changing from Ar to CO_2. The maximum cathodic current under CO_2 is found at –3.03 V(*vs*. Fc^+/Fc), and the ratio of the cathodic currents is $\frac{i_{cat}(CO_2)}{i_{cat}(Ar)} = 11.3$, the highest of the neutral complexes herein described.

The anodic scan of **4d**, shown in Figure S17, deserves some comment, since an additional irreversible wave appears at lower potential (see also Table 2). The origin of this new wave with an $E_{pk}^{ox} = 0.39\ V$ (*vs*. Fc^+/Fc) may be associated to the possibility of a higher proton-resonance effect, between the protonated and deprotonated pypz ligands. In fact, in this complex the remaining proton may be delocalized among three nitrogen donor atoms, instead of two nitrogen atoms for the rest of neutral complexes **4a-c**. The maximum cathodic current under CO_2 is found for **4d** at –3.03 V(*vs*. Fc^+/Fc), and the ratio of the cathodic currents is $\frac{i_{CO_2}}{i_{Ar}} = 9.7$ at this potential.

As for **1**, the electrochemistry of **5d** under N_2 at a platinum electrode using the SCE reference electrode in THF has been previously studied,[19] whereas herein is included the electrochemistry at a GC (glassy carbon) electrode in dry MeCN using the AgCl/Ag reference electrode. Two single-electron irreversible oxidations wave at E_{pk}^{ox} = 0.97 and 1.30 V vs. SCE were detected under Pt/THF.[19] We now observe under GC/MeCN (Figure S18 and Table S4) three one-electron irreversible oxidations at E_{pk}^{ox} = 0.78, 0.98, 1.40 V vs. AgCl/Ag (NaCl, 3M). One one-electron reduction is detected when scanning to negative potentials under Ar, and an intense enhancement of the cathodic current is observed when repeating the same scan under CO_2 (Figure S18). The maximum cathodic current under CO_2 is found at –2.77 V (vs. Fc^+/Fc), and the ratio of the cathodic current is $\frac{i_{CO_2}}{i_{Ar}} = 5.6$, at this potential. As shown in Table 2, the electrochemical properties of **5d** are very similar to those of its protonated parent **4d**,

although the main difference is precisely their behavior under CO_2, where the ratio of the cathodic current is higher for the neutral complex **4d** (9.7). This similarity may be explained considering the structural analogy between the neutral complex **4d** and its deprotonated form **5d** (Figure 5), where a covalently bonded sodium atom may be proposed, according to the crystal structures of the manganese(I) complexes [{*fac*-Mn(CO)$_3$(μ^2-pypz)(μ-pypz)M}$_n$] (M = Li, n =1; M = Na, K; n =2), which could be crystallographically characterized.[19] In fact, the main electrochemical difference between **4d** and **4d** is precisely their behavior under CO_2, where the ratio of the cathodic current is higher for the neutral complex **4d** (9.7 *vs*. 5.6 for **5d**). This is in accocdance with the relevance of the presence of protons in the electrochemical reduction of CO_2. The lower stability of the other complexes **5a-c** may be related to their prominent anionic nature, as depicted in Figure 2.

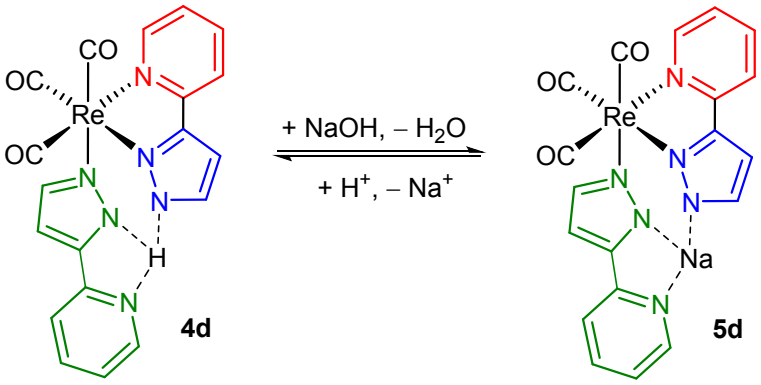

Figure 5. Complexes *fac*-[Re(CO)$_3$(pypzH)(pypz)] (**4d**) and Na[*fac*-Re(CO)$_3$(pypz)$_2$] (**5d**).

Cationic complexes **3a-d** display similar results of the anodic scans. A clean and apparently reversible wave at +1.42 V assigned to one-electron transfer Re(I) to Re(II) is detected for **3a**, as shown in Figures S6 and S7. This wave is not affected by the change from Ar to CO_2 atmosphere (the blue and red traces overlap completely), indicating a pure electron transfer reaction. The observed reversibility may be understood in terms of the proposed mechanism by Bullock et al.[28] According to this mechanism, a ligand bridges two Re(II) units

following the electron transfer, but cationic complexes **3a-c** do not contain a ligand able to bridge two metal atoms, thus avoiding the chemical step that follows the electron transfer. On the contrary, neutral complexes **4a-d** do contain an available lone pair in the pyridylpyrazolate ligand to behave as bridging ligand, and thus they follow the expected pattern. Going to reduction potentials, four peaks are observed at –1.94, –2.30, –2.74, –2.89 V (210 μA) under Ar. However, under CO_2 only two peaks at –1.73 V and –2.09 V remain observable, since the peaks at more negative potentials are hidden by the catalytically enhanced current. This means that reduction of CO_2 only starts when the complex has been reduced by, at least, two electrons. The observation that the peak of the enhanced current does not reach a plateau is another particular feature of **3a**. Such plateau current may be unveiled at lower concentration of CO_2. Figure S7 displays the evolution of the CV's when the concentration of CO_2 is progressively reduced by bubbling Ar: under saturated CO_2 a current value of 2200 μA without plateau was recorded (Figure S6), but removing CO_2 by bubbling Ar for 3 min (Figure S7, black trace) the current value obtained is 612 μA, at 5 min (Figure S7, red trace) is reduced to 447 μA and after 7 min (Figure S7, blue trace) to 262 μA, a close value to the current observed under Ar (210 μA, Figure S6). A similar experiment on **3b** is shown in Figure S11. For **3a**, the maximum cathodic current under CO_2 is found at –3.03 V(*vs*. Fc^+/Fc), and the ratio of the cathodic currents is $\frac{i_{CO_2}}{i_{Ar}} = 6.5$ at this potential.

For **3b**, the scan to positive potentials (Figures S8 and S9) shows a "quasi-reversible" wave at +1.40 V assigned to one-electron transfer $Re^{I} \rightarrow Re^{II}$. This wave is not affected by the change form Ar to CO_2 (the black and red traces overlap completely in Figure S9) indicating a pure electron transfer reaction. This complex has been selected to illustrate (Figure S10) how potentials and currents are perturbed by the presence of ferrocene, which is used as internal reference calibrant at the end of each electrochemical measurement. In addition, this

experiment allows to compare the results under the silver wire pseudoreference electrode (Figures S8 and S9) or the AgCl/Ag (3M NaCl) reference electrode (Figure S10).

Complex **3c** shows (Figure S12) the greatest current enhancement ratio ($\frac{i_{CO_2}}{i_{Ar}} = 11.5$) for all the complexes herein reported, a value close to that shown by the corresponding neutral complex **4c** (11.3). This suggests that the presence of indazole ligand in the sixth coordination position might play a main role in the reduction mechanism of the CO_2. This feature may be explained considering the acidity of the pyrazole ligand, as detailed below.

Finally, complex **3d** shows a peculiar feature at oxidative or anodic scans (Figure S13). The pattern reminds that of the neutral complexes **4a-c** discussed above. Complex **3d** is the only cationic example with a free donor nitrogen atom able to bridge two rhenium atoms in order to follow the proposed mechanism by Bullock et al.[28]

The accepted mechanism for the electrocatalytic reduction of CO_2 with Mn(I) and Re(I) tricarbonyl complexes starts with the dissociation of the "sixth" ligand from the one-reduced-electron complex, generating a 17 electron species that binds CO_2.[6] In our system, the "sixth" coordination position is occupied by different pyrazole ligands, therefore determining the strengh of their bonds to the metal is crucial in order to explain the enhancement of the current observed for CO_2 atmosphere. Thus, the energies of the different Re-pz*H bonds have been calculated both the for cationic complexes and for their one-reduced-electron species (Figure S19 and Table S5). The results indicate that bond energies of the one-reduced-electron species (from 3.4 to 7.6 Kcal/mol) are much lower than those of the cationic complexes (from 23.9 to 25.2 Kcal/mol), supporting that dissociation of the "sixth" ligand is facilitated once the complex has been reduced. However, the values obtained (Table S5) do not depend on the nature of the pyrazole, what does not allow to explain the differences observed between the cationic compounds. This contrasts with the experimental values, since as indicated above, complexes containing indazole show the highest catalytic

activity (11.5 or 11.3 for **3c** or **4c** respectively *vs*. 7.2 for the related bromido complex **1**, see Table 2). But this observation might be related to the second step in the catalytic process, where the η^1-C-bound CO_2 is activated by proton donors, so C−O bond cleavage is facilitated.[6c] Therefore, a higher acidity of the uncoordinated pyrazole might promote this second step, and in fact the values obtained for the catalytic activity in the electrocatalytic reduction of CO_2 are similar to those reported for the acidity of pyrazoles experimentally determined (indzH > pzH > dmpzH, no pypzH nor 3-phenylpyrazole were included in these studies).[22] In conclusion, one determining factor in order to explain the different behavior of the complexes herein described as catalysts for CO_2 reduction might be related to the acidity of the pyrazoles coordinated in the "sixth" position, which after being liberated, may activate the coordinated CO_2 once the first one-electron-reduction occurs. The lower catalytic activity of **5d**, which is the only complex without protons, also supports this proposal.

CONCLUSIONS

Cationic rhenium(I) tricarbonyl complexes containing pypzH as chelate ligand and different pyrazoles pz*H as monodentate ligands have been synthesized and successively deprotonated in order to obtain the corresponding neutral and anionic complexes. The latter are too unstable both in the solid state and in solution, what precluded the study. The first deprotonation occurs formally on the pypzH ligand, even though the remaining proton is delocalized in solution among the basic nitrogen atoms of the pyrazolyl groups. The luminiscent and electrochemical properties of the cationic, neutral and one of the anionic complexes have been studied in order to determine the influence of the deprotonation process on these properties. The luminescent properties of the complexes herein described is similar to related *fac*-$Re^I(CO)_3$ species, as well as their behavior in acid-base processes, in some cases with

significative decreases of quatum yields as protons are removed. The complexes are active in the electrocatalyzed reduction of CO_2, some of the catalytic activities being higher than those reported for similar bromido complexes. In fact, the catalytic activity of the complexes herein reported might be related to the acidity of the pyrazoles coordinated in the "sixth" position.

EXPERIMENTAL

General remarks. All manipulations were performed under a N_2 atmosphere following conventional Schlenk techniques. Solvents were purified according to standard procedures.[34] Compounds **1**,[15] and **5d**,[19] were obtained as previously described. All other reagents were obtained from the usual commercial suppliers, and used as received. Infrared spectra were recorded in a Perkin-Elmer RX I FT-IR apparatus using 0.2 mm CaF_2 cells for solutions or in a Bruker Tensor 27 FTIR for solid samples. NMR spectra were recorded in a Agilent MR 400 or in a Agilent 500 DD2 instruments in $(CD_3)_2CO$ at room temperature (r.t.) unless otherwise indicated, and are referred to the internal residual solvent peak for ^1H and $^{13}C\{1H\}$ NMR. Assignment of the ^1H NMR spectra (Figure 6) was supported by COSY, TOCSY and NOESY experiments and assignment of $^{13}C\{^1H\}$ NMR data was supported by HMBC and HSQC heteronuclear experiments. Elemental analyses were performed on a Thermo Fisher Scientific EA Flash 200.

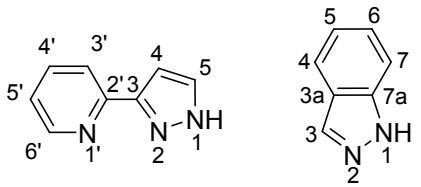

Figure 6. Numbering of pypzH and indzH for NMR assignment.

***fac*-[Re(CO)$_3$(pzH)(pypzH)]OTf, 3a**.

AgOTf (0.152 g, 0.6 mmol) was added to a solution of **1** (0.245 g, 0.5 mmol) in THF (20 mL), the mixture was stirred at r.t. for 1 h in the absence of light, and then filtered to remove solid AgBr. Removal of the solvent *in vacuo* gave **2** as an orange oil.[35] This oil was dissolved in THF (25 mL), pzH was added (0.034 g, 0.5 mmol) and the solution was stirred at 40 ºC for 24 h. The solution was concentrated *in vacuo*, and Et_2O was added (*ca*. 25 mL). Cooling al –20 ºC gave a yellow microcrystalline solid, which was decanted, washed with Et_2O (3 × 3 mL), and dried, yielding 0.230 g (73 %). ^{1}H NMR (500 MHz) δ: 6.38 (t, J = 2.4 Hz, H^4 pzH 1 H), 7.25 (d, J = 2.3 Hz, $H^{3,5}$ pzH, 1 H), 7.45 (d, J = 2.6 Hz, H^5 pypzH, 1 H), 7.77 (ddd, J = 7.3, 5.5, and 1.8 Hz, $H^{5'}$ pypzH, 1 H), 7.97 (d, J = 2.6 Hz, $H^{5,3}$ pzH, 1 H), 8.31-8.53 (m, H^4, $H^{3'}$ and $H^{4'}$ pypzH, 3 H), 9.27 (d, J = 5.4 Hz, $H^{6'}$ pypzH, 1 H), 12.94 (br s, N*H* pzH, 1 H), 14.18 (br s, N*H* pypzH, 1 H). ^{13}C{^{1}H} NMR (101 MHz) δ: 105.7 (C^5 pypzH), 107.1 (C^4 pzH), 123.3 ($C^{3'}$ pypzH), 127.0 ($C^{5'}$ pypzH), 132.9 ($C^{5,3}$ pzH), 135.4 (C^4 pypzH), 141.3 ($C^{4'}$ pypzH), 141.9 ($C^{3,5}$ pzH), 151.2 ($C^{2'}$ pypzH), 153.9 (C^3 pypzH), 154.2 ($C^{6'}$ pypzH), *C*O not detected, all signals are singlets. IR (THF, cm^{-1}): 2035 vs, 1935 s, 1920 vs. IR (solid, cm^{-1}): 3146 w, 2031 vs, 1918 vs, 1616 w, 1440 w, 1367 w, 1284 m, 1240 s, 1222 s, 1159 s, 1138 m, 1094 m, 1067 s, 1051 s, 1026 s, 910 w, 885 w, 802 w, 764 m, 634 m. Anal. Calcd for $C_{15}H_{11}F_3N_5O_6ReS$: C, 28.48; H, 1.75; N, 11.07. Found: C, 28.67; H, 1.84; N, 11.14.

***fac*-[Re(CO)$_3$(dmpzH)(pypzH)]OTf, 3b**

The oil containing **2** (0.5 mmol) obtained as indicated for **3a** was dissolved in THF (25 mL), dmpzH was added (0.048 g, 0.5 mmol) and the solution was stirred at 40 ºC for 24 h. Work up as for **3a** gave **3b** as a pale brown microcrystalline solid. Yield 0.230 g (73 %). ^{1}H NMR (400 MHz) δ: 2.07 (s, CH_3 dmpzH, 3 H), 2.09 (s, CH_3 dmpzH, 3 H), 5.93 (s, H^4 dmpzH, 1 H), 7.36 (d, J = 1.9 Hz, H^5 pypzH, 1 H), 7.79 (m, $H^{5'}$ pypzH, 1 H), 8.33 (m, $H^{3'}$, $H^{4'}$ and H^4 pypzH, 3

H), 9.39 (d, J = 4.3 Hz, $H^{6'}$ pypzH, 1 H), 11.58 (br s, N*H* dmpzH, 1 H), 14.17 (br s, N*H* pypzH, 1 H). $^{13}C\{^1H\}$ NMR (101 MHz) δ: 9.5 ($C^{5,3}H_3$ dmpzH), 13.9 ($C^{3,5}H_3$ dmpzH), 106.7 (C^5 pypzH), 107.8 (C^4 dmpzH), 124.2 ($C^{3'}$ pypzH), 127.6 ($C^{5'}$ pypzH), 136.1 (C^4 pypzH), 142.3 ($C^{4'}$ pypzH), 145.1 ($C^{5,3}$ dmpzH), 152.4 ($C^{2'}$ pypzH), 154.5 ($C^{3,5}$ dmpzH), 155.0 (C^3 pypzH), 155.8 ($C^{6'}$ pypzH), *C*O not detected, all signals are singlets. IR (THF, cm^{-1}): 2035 vs, 1937 s, 1918 vs. IR (solid, cm^{-1}): 3371 w, 3155 w, 3038 w, 2963 w, 2931 w, 2029 vs, 1910 vs br, 1617 w, 1578 w, 1439 w, 1372 w, 1294 m, 1280 m, 1238 m, 1222 m, 1210 m, 1165 m, 1152 m, 1118 w, 1027 s, 817 w, 772 m, 632 s. Anal. Calcd for $C_{17}H_{15}F_3N_5O_6ReS$: C, 30.91; H, 2.29; N, 10.60. Found: C, 31.07; H, 2.12; N, 10.30.

***fac*-[Re(CO)$_3$(indzH)(pypzH)]OTf, 3c**

The oil containing **2** (0.5 mmol) obtained as indicated for **3a** was dissolved in THF (25 mL), indzH was added (0.059 g, 0.5 mmol) and the solution was stirred at 40 ºC for 24 h. Work up as for **3a** gave **3c** as a yellow microcrystalline solid. Yield 0.326 g (95 %). ^1H NMR (500 MHz) δ: 7.19 (dd, J = 8.1 and 6.6 Hz, H^6 indzH, 1 H), 7.42 (d, J = 1.9 Hz, H^5 pypzH, 1 H), 7.50 (m, H^5 and H^4 indzH, 2 H), 7.66 (d, J = 8.1 Hz, H^7 indzH, 1 H), 7.79 (t, J = 5.6 Hz, $H^{5'}$ pypzH, 1 H), 7.89 (s, H^3 indzH, 1 H), 8.37 (m, H^4, $H^{3'}$ and $H^{4'}$ pypzH, 3 H), 9.32 (d, J = 5.6 Hz, $H^{6'}$ pypzH, 1 H), 12.93 (sa, N*H* indzH, 1 H), 14.20 (sa, N*H* pypzH, 1 H). $^{13}C\{^1H\}$ NMR (101 MHz) δ: 105.9 (C^5 pypzH), 110.2 (C^4 indzH), 120.9 (C^7 indzH), 122.3 (C^{7a} indzH), 122.7 (C^6 indzH), 123.4 ($C^{3'}$ pypzH), 127.1 ($C^{5'}$ pypzH), 129.6 (C^5 indzH), 135.6 (C^4 pypzH), 137.6 (C^3 indzH), 141.3 (C^{3a} indzH), 141.4 ($C^{4'}$ pypzH), 151.3 ($C^{2'}$ pypzH), 154.0 (C^3 pypzH), 154.3 ($C^{6'}$ pypzH), *C*O not detected, all signals are singlets. IR (THF, cm^{-1}): 2037 vs, 1938 s, 1922 vs. IR (solid, cm^{-1}): 3167 w, 2031 vs, 1933 vs br, 1630 w, 1618 w, 1439 w, 1285 m, 1241 m, 1224 m, 1154 m, 1125 m, 1092 w, 1050 s, 1027 s, 1003 s, 867 w, 773 m,

745 m, 700 w, 630 m. Anal. Calcd for $C_{19}H_{13}F_3N_5O_6ReS$: C, 33.43; H, 1.92; N, 10.26. Found: C, 33.60; H, 2.06; N, 10.11.

***fac*-[Re(CO)$_3$(pypzH-*κ*^{1}*N*)(pypzH-*κ*^{2}*N,N*)]OTf, 3d**

The oil containing **2** (0.5 mmol) obtained as indicated for **3a** was dissolved in THF (25 mL), pypzH was added (0.073 g, 0.5 mmol) and the solution was stirred at 40 ºC for 24 h. The volatiles were removed *in vacuo* and the resulting yellow oil was crystallized in CH_2Cl_2/Et_2O at –20 ºC giving a pale yellow microcrystalline solid, which was decanted, washed with Et_2O (3 × 3 mL), and dried, yielding 0.285 g (80 %). ^{1}H NMR (400 MHz) δ: 6.90 (s, *H*^{5} pypzH-*N*, 1 H), 7.28 (s, *H*^{4} pypzH-*N*, 1 H), 7.42 (m, *H*$^{5'}$ pypzH-*N*, 1 H), 7.44 (d, J = 2.6 Hz, *H*^{5} pypzH-*N,N*, 1 H), 7.82 (d, J = 5.8 Hz, *H*$^{5'}$ pypzH-*N,N*, 1 H), 7.85 (d, J = 7.6 Hz, *H*$^{3'}$ pypzH-*N*, 1 H), 7.89 (d, J =7.6 Hz, *H*$^{4'}$ pypzH-*N*, 1 H), 8.37 (d, J = 2.6 Hz, *H*^{4} pypzH-*N,N*, 1 H), 8.38 (m, *H*$^{4'}$ pypzH-*N,N*, 1 H), 8.41 (s, *H*$^{3'}$ pypzH-*N,N*, 1 H), 8.59 (d, J = 3.7 Hz, *H*$^{6'}$ pypzH-*N*, 1 H), 9.32 (d, J = 5.8 Hz, *H*$^{6'}$ pypzH-*N,N*, 1 H), 12.94 (br s, N*H*, 1 H), 14.06 (br s, N*H*, 1 H). ^{13}C{^{1}H} NMR (101 MHz) δ: 105.5 (*C*^{5} pypzH-*N*), 105.8 (*C*^{5} pypzH-*N,N*), 121.2 (*C*$^{3'}$ pypzH-*N*), 123.4 (*C*$^{3'}$ pypzH-*N,N*), 124.4 (*C*$^{5'}$ pypzH-*N*), 126.9 (*C*$^{5'}$ pypzH-*N,N*), 135.4 (*C*^{4} pypzH-*N,N*), 137.5 (*C*$^{4'}$ pypzH-*N*), 141.3 (*C*$^{4'}$ pypzH-*N,N*), 143.2 (*C*^{4} pypzH-*N*), 145.9 (*C*$^{2',3}$ pypzH-*N*), 145.9 (*C*$^{3,2'}$ pypzH-*N*), 149.7 (*C*$^{6'}$ pypzH-*N*), 151.3 (*C*$^{2'}$ pypzH-*N,N*), 154.0 (*C*^{3} pypzH-*N,N*), 154.4 (*C*$^{6'}$ pypzH-*N,N*), *C*O not detected, all signals are singlets. IR (THF, cm^{-1}): 2036 vs, 1934 s, 1921 vs. IR (solid, cm^{-1}): 3157 w, 2033 vs, 1912 vs br, 1615 w, 1456 w, 1432 w, 1274 m, 1242 s, 1223 s, 1154 m, 1104 w, 1093 w, 1056 w, 1027 w, 994 s, 970 s, 805 s, 775 s, 709 w, 632 s. Anal. Calcd for $C_{20}H_{14}F_3N_6O_6ReS$: C, 33.85; H, 1.99; N, 11.84. Found: C, 33.98; H, 1.88; N, 11.74.

***fac*-[Re(CO)$_3$(pzH)(pypz)], 4a**.

Na_2CO_3 (0.064 g, 0.6 mmol) is added to a solution of **3a** (0.127 g, 0.2 mmol) in THF (10 mL), and the mixture is stirred at r.t. for 1 h. The reaction mixture was filtered, and hexane (*ca*. 20 mL) was added to the filtrate. The solution was concentrated and cooled to −20 °C, giving a pale yellow microcrystalline solid, which was decanted, washed with hexane (3 × 3 mL approximately), and dried *in vacuo*, yielding 0.060 g (62%). ^{1}H NMR (500 MHz) δ: 6.27 (t, J = 2.4 Hz, H^4 pzH, 1 H), 6.81 (d, J = 1.9 Hz, H^5 pypz, 1 H), 7.29 (d, J = 2.2 Hz, $H^{3,5}$ pzH, 1 H), 7.44 (ddd, J = 7.3, 5.6, and 1.4 Hz, $H^{5'}$ pypz, 1 H), 7.58 (d, J = 2.0 Hz, H^4 pypz, 1 H), 7.80 (d, J = 2.6 Hz, $H^{5,3}$ pzH, 1 H), 7.91 (d, J = 8.0 Hz, $H^{3'}$ pypz, 1 H), 8.09 (td, J = 7.8 and 1.5 Hz, $H^{4'}$ pypz, 1 H), 9.09 (dt, J = 5.6 and 1.3 Hz, $H^{6'}$ pypz, 1 H), N*H* not detected. ^{13}C{^{1}H} NMR (101 MHz) δ: 104.4 (C^5 pypz), 107.3 (C^4 pzH), 120.9 ($C^{3'}$ pypz), 123.5 ($C^{5'}$ pypz), 132.6 ($C^{5,3}$ pzH), 140.8 ($C^{4'}$ pypz), 142.5 ($C^{3,5}$ pzH), 143.0 (C^4 pypz), 153.4 ($C^{6'}$ pypz), 151.2 (C^3 pypz), 155.4 ($C^{2'}$ pypz), *C*O not detected, all signals are singlets. IR (THF, cm^{-1}): 2021 s, 1914 s, 1900 s. IR (solid, cm^{-1}): 3676 w, 3571 w, 2961 w, 2914 w, 2018 s, 1885 s br, 1609 m, 1536 m, 1482 w, 1456 w, 1430 w, 1371 w, 1350 w, 1257 s, 1232 s, 1171 s, 1035 s, 978 w, 942 w, 901 w, 879 w, 843 w, 801 w, 778 m, 765 m, 750 w, 709 w, 631 s, 588 w, 537 w, 516 m, 490 w, 477 w, 422 m. Anal. Calcd for $C_{14}H_{10}N_5O_3Re$: C, 34.85; H, 2.09; N, 14.52. Found: C, 34.68; H, 2.14; N, 14.33.

***fac*-[Re(CO)$_3$(dmpzH)(pypz)], 4b**.

The same procedure as for **4a**, using **3b** (0.132 g, 0.2 mmol) as starting material, gave 0.061 g (60%) of **4b** as an white-yellow microcrystalline solid. ^{1}H NMR (400 MHz) δ: 2.05 (s, CH_3 dmpzH, 3 H), 2.19 (s, CH_3 dmpzH, 3 H), 5.82 (s, H^4 dmpzH, 1 H), 6.74 (d, J = 2.1 Hz, H^5 pypz, 1 H), 7.37 (dd, J = 7.5 and 5.8 Hz, $H^{5'}$ pypz, 1 H), 7.64 (d, J = 2.1 Hz, H^4 pypz, 1 H), 7.82 (d, J = 7.5 Hz, $H^{3'}$ pypz, 1 H), 8.02 (t, J = 7.5 Hz, $H^{4'}$ pypz, 1 H), 9.08 (d, J = 5.8 Hz, $H^{6'}$ pypz, 1 H), 10.38 (br s, N*H* dmpzH, 1 H). ^{13}C{^{1}H} NMR (101 MHz) δ: 9.7 (CH$_3$ dmpzH),

13.7 (CH_3 dmpzH), 104.1 (C^5 pypz), 106.2 (C^4 dmpzH), 120.3 ($C^{3'}$ pypz), 122.6 ($C^{5'}$ pypz), 139.9 ($C^{4'}$pypz), 142.0 ($C^{5,3}$ dmpzH), 143.0 (C^4 pypz), 152.2 (C^3 pypz), 152.3 ($C^{3,5}$ dmpzH), 153.0 ($C^{6'}$ pypz), 155.6 ($C^{2'}$ pypz), 194.1 (CO), 195.9 (CO), 198.0 (CO), all signals are singlets. IR (THF, cm^{-1}): 2021 s, 1916 s, 1897 s. IR (solid, cm^{-1}): 3899 w, 3272 m, 2961 w, 2853 w, 2012 s, 1886 vs br, 1610 m, 1573 m, 1539 m, 1454 m, 1419 m, 1376 m, 1346 m, 1259 m, 1201 m, 1156 m, 1146 m, 1127 m, 1096 m, 1049 m, 1017 m, 972 m, 929 m, 799 m, 754 s, 698 m, 629 m, 614 m, 546 m, 538 m, 491 m, 476 m. Anal. Calcd for $C_{16}H_{14}N_5O_3Re$: C, 37.64; H, 2.76; N, 13.72. Found: C, 37.51; H, 2.95; N, 13.94.

***fac*-[Re(CO)$_3$(indzH)(pypz)], 4c**.

The same procedure as for **4a**, using **3c** (0.132 g, 0.2 mmol) as starting material, gave 0.063 g (59%) of **4c** as an white-yellow microcrystalline solid. ^{1}H NMR (400 MHz) δ: 6.74 (s, H^5 pypz, 1 H), 7.13 (m, H^5 indzH, 1 H), 7.31 (t, J = 6.0 Hz, $H^{5'}$ pypz, 1 H), 7.41 (m, H^6 indzH, 1 H), 7.55 (d, J = 8.9 Hz, H^7 indzH, 1 H), 7,59 (s, H^4 pypz, 1 H), 7.65 (d, J = 11.1 Hz, H^4 indzH, 1 H), 7.68 (s, H^3 indzH, 1 H), 7.78 (d, J = 8.3 Hz, $H^{3'}$ pypz, 1 H), 7.98 (dd, J = 8.3 and 6.0 Hz, $H^{4'}$ pypz, 1 H), 9.02 (d, J = 6.0 Hz, $H^{6'}$ pypz, 1 H), NH not detected. ^{13}C{^{1}H} NMR (101 MHz) δ: 103.7 (C^5 pypz), 110.2 (C^7 indzH), 120.0 ($C^{3'}$ pypz), 120.2 (C^5 indz), 120.8 (C^4 indzH), 122.2 (C^{3a} indzH), 122.6 ($C^{5'}$ pypz), 128.9 (C^6 inzH), 137.2 (C^3 indzH), 139.9 ($C^{4'}$ pypz), 140.8 (C^{7a} indzH), 142.4 (C^4 pypz), 152.6 ($C^{6'}$ pypz), 155.3 (C^3 pypz), 155.6 ($C^{2'}$ pypz), CO not detected, all signals are singlets. IR (THF, cm^{-1}): 2022 s, 1918 s, 1900 s. IR (solid, cm^{-1}): 3675 w, 3155 w, 2962 m, 2017 s, 1895 s br, 1611 m, 1538 w, 1503 w, 1457 w, 1431 w, 1388 w, 1355 w, 1257 s, 1232 m, 1172 s, 1079 s, 1033 s, 952 w, 869 w, 845 w, 795 s, 762 m, 741 m, 707 w, 631 m, 587 w, 534 m, 515 w, 476 w, 428 m. Anal. Calcd for $C_{18}H_{12}N_5O_3Re$: C, 40.60; H, 2.27; N, 13.15. Found: C, 40.44; H, 2.08; N, 13.04.

***fac*-[Re(CO)$_3$(pypzH-*κ*^{1}*N*)(pypz-*κ*^{2}*N,N*)], 4d**

The same procedure as for **4a**, using **3d** (0.132 g, 0.2 mmol) as starting material, gave 0.055 g (49%) of **4d** as a pale yellow microcrystalline solid. ^{1}H NMR (400 MHz) δ: 6.53 (s, *H*^{5} pypz-*N,N*, 1 H), 6.67 (s, *H*^{5} pypzH-*N*, 1 H), 7.16 (s, *H*$^{5'}$ pypzH-*N*, 1 H), 7.30 (m, *H*^{4} pypz-*N,N*, 1 H), 7.33 (m, *H*$^{5'}$ pypz-*N,N*, 1 H), 7.51 (m, *H*^{4} pypzH-*N*, 1 H), 7.55 (m, *H*$^{3'}$ pypzH-*N*, 1 H), 7.71 (m, *H*$^{4'}$ pypzH-*N*, 1 H), 7.73 (m, *H*$^{3'}$ pypz-*N,N*, 1 H), 7.94 (t, J = 7.8 Hz, *H*$^{4'}$ pypz-*N,N*, 1 H), 8.41 (s, *H*$^{6'}$ pypzH-*N*, 1 H), 9.04 (d, J = 5.6 Hz, *H*$^{6'}$ pypz-*N,N*, 1 H), N*H* not detected. ^{13}C{^{1}H} NMR (101 MHz) δ: 102.1 (*C*^{5} pypz-*N,N*), 102.8 (*C*^{5} pypzH-*N*), 103.2 (*C*^{4} pypz-*N,N*), 119.5 (*C*$^{3'}$ pypzH-*N*), 119.8 (*C*$^{3'}$ pypz-*N,N*), 120.9 (*C*$^{2'}$ pypzH-*N*), 122.3 (*C*$^{5'}$ pypz-*N,N*), 136.9 (*C*$^{4'}$ pypzH-*N*), 139.1 (*C*$^{4'}$ pypz-N,N), 140.3 (*C*^{3} pypz-*N,N*), 141.7 (*C*^{4} pypzH-*N*), 148.9 (*C*$^{5'}$ pypzH-*N*), 149.2 (*C*$^{6'}$ pypzH-*N*), 151.4 (*C*^{3} pypzH-*N*), 151.9 (*C*$^{6'}$ pypz-*N,N*), 155.9 (*C*$^{2'}$ pypz-*N,N*), *C*O not detected, all signals are singlets. IR (THF, cm^{-1}): 2021 s, 1918 s, 1896 s. IR (solid, cm^{-1}): 2973 w, 2932 w, 2006 vs, 1880 vs, 1868 vs, 1696 m, 1612 m, 1592 m, 1565 m, 1536 m, 1512 m, 1454 m, 1427 m, 1347 m, 1149 m, 1128 m, 1118 m, 1089 m, 1056 m, 972 w, 946 w, 761 s, 708 m, 643 m, 627 m. Anal. Calcd for $C_{19}H_{13}N_6O_3Re$: C, 40.78; H, 2.34; N, 15.02. Found: C, 40.52; H, 2.19; N, 14.72.

Na[*fac*-{Re(CO)$_3$(pz)(pypz)}], 5a.

Method A: **3a** (0.006 g, 0.01 mmol) was dissolved in $(CD_3)_2CO$ or THF (0.5 mL) and 0.025 mL of 1 M NaOH solution (0.025 mmol) in D_2O or H_2O was added. *Method B:* **4a** (0.005 g, 0.01 mmol) and 0.012 mL of 1 M NaOH solution (0.012 mmol) was added. The compound was not isolated. ^{1}H NMR (500 MHz) δ: 8.84 (m, *H*^{4} pzH, 1 H), 6.65 (d, J = 1.9 Hz, *H*^{5} pypz, 1 H), 6.91 (d, J = 2.0 Hz, *H*^{3,5} pzH, 1 H), 7.28 (m, *H*$^{5'}$ and *H*^{4} pypz, 2 H), 7.48 (d, J = 1.9 Hz, *H*^{5,3} pzH, 1 H), 7.72 (dt, J = 8.0 and 1.2 Hz, *H*$^{3'}$ pypz, 1 H), 7.93 (td, J = 7.7 and 1.6 Hz, *H*$^{4'}$

pypz, 1 H), 9.01 (dt, J = 5.6 and 1.3 Hz, $H^{6'}$ pypz, 1 H). IR (THF, cm^{-1}): 2007 s, 1896 s, 1880 s.

Na[*fac*-{Re(CO)$_3$(dmpz)(pypz)}], 5b.

Method A: **3b** (0.007 g, 0.01 mmol) was dissolved in $(CD_3)_2CO$ or THF (0.5 mL) and 0.025 mL of 1 M NaOH solution (0.025 mmol) in D_2O or H_2O was added. *Method B:* **4b** (0.005 g, 0.01 mmol) and 0.012 mL of 1 M NaOH solution (0.012 mmol) was added. The compound was not isolated. ^{1}H NMR (400 MHz) δ: 1.85 (s, CH_3 dmpzH, 3 H), 1.91 (s, CH_3 dmpzH, 3 H), 5.20 (s, H^4 dmpzH, 1 H), 6.53 (s, H^5 pypz, 1 H), 7.21 (t, J = 4.5 Hz, $H^{5'}$ pypz, 1 H), 7.43 (s, H^4 pypz, 1 H), 7.58 (d, J = 5.5 Hz, $H^{3'}$ pypz, 1 H), 7.82 (t, J = 5.5 Hz, $H^{4'}$ pypz, 1 H), 9.13 (d, J = 3.5 Hz, $H^{6'}$ pypz, 1 H). IR (THF, cm^{-1}): 2009 s, 1898s, 1885s.

Na[*fac*-{Re(CO)$_3$(indz)(pypz)}], 5c.

Method A: **3c** (0.007 g, 0.01 mmol) was dissolved in $(CD_3)_2CO$ or THF (0.5 mL) and 0.025 mL of 1 M NaOH solution (0.025 mmol) in D_2O or H_2O was added. *Method B:* **4c** (0.005 g, 0.01 mmol) and 0.012 mL of 1 M NaOH solution (0.012 mmol) was added. The compound was not isolated. ^{1}H NMR (500 MHz) δ: 6.73 (s, H^5 pypz, 1 H), 6.96 (m, H^5 indzH, 1 H), 7.22 (m, $H^{5'}$ pypz, 1 H), 7.38 (m, H^6 indzH, 1 H), 7.46 (d, J = 10 Hz, H^7 indzH, 1 H), 7,56 (m, H^4 pypz and H^4 indzH, 2 H), 7.65 (m, H^3 indzH, 1 H), 7.80 (d, J = 7 Hz, $H^{3'}$ pypz, 1 H), 7.99 (m, $H^{4'}$ pypz, 1 H), 9.15 (d, J = 4.0 Hz, $H^{6'}$ pypz, 1 H). IR (THF, cm^{-1}): 2009 s, 1898 s, 1884 s.

Photophysical studies

The solvents for spectroscopic studies were of spectroscopic grade and used as received. Ultraviolet–visible (UV–Vis) and fluorescence spectra were recorded in optically dilute solutions (from 10^{-5} M to 5×10^{-5} M), at room temperature with a quartz cuvette (1 cm×1 cm),

using a Hitachi U-3900 and an F-7000 Hitachi Fluorescence spectrophotometers, respectively. Fluorescence decay lifetimes were measured in deaerated solvents, using a time-correlated single photon counting instrument (FLS980 Series, Edinburgh instruments) with a 405 nm pulsed LED (Edinburgh instruments, EPL-510) light source having a 50–500 ns at r.t. The absolute fluorescence quantum yields in each solvent were measured using the integrating sphere accessory with a FLS980 Series Edinburgh instrument at r.t., wherein the solvent was used as a reference.

Electrochemical studies

Electrochemical measurements were carried out with Dropsens μStat 400 (range –4V to +4V, software DropView 8400 Version 2.2) or Dropsens μStat 300 (range –2V to +2V) or PalmSens 3 potentiostats (range –5V to +5V, software PSTrace4 Version 4.4.2). Unless otherwise stated CV's were scanned at 200 mVs−1, in MeCN (5 mL), 0.1M $^{n}Bu_4PF_6$ supporting electrolyte, purging with Ar or CO_2 at room temperature through a PTFE tubing. Working electrodes were of glassy carbon (3 mm diameter). The auxiliary electrode was a platinum wire. The reference electrodes used were Ag/AgCl (3M NaCl) MF-2052 BASi (separated from the bulk solution by a "thirsty" Vycor™ frit) or a silver wire pseudo-reference electrode. Ferrocene was added at the end of each experiment. The observed ferrocenium/ferrocene couple was $E_{1/2}$ = 0.443± 0.005 V vs. Ag/AgCl. Potential values measured with the Ag wire are plenty of uncertainty and, at the end of the experiment, measures must be carried out with the Ag/AgCl (3M NaCl) electrode. The solubility of saturated CO_2 in MeCN has been reported to be 0.28M at 25°C.[36] Changing atmosphere from pure Ar to pure CO_2 or *vice versa* required bubbling with the new gas for not less than 5 minutes. Lasting such time the CV's obtained were the same than those obtained in the first scan under a specific atmosphere. Bubbling was kept during the interim between scans.

During scan time the PTFE was risen and kept above the surface of the solution to avoid agitation.

Computational details

All calculations have been performed using the Gaussian 16 program package,[37] in which the B3LYP functional was used.[38] Geometry optimizations were performed under no symmetry restrictions, using initial coordinates derived from X-ray data of the same complexes when availables, and frecuency analyses were performed to ensure that a minimum structure with no imaginary frecuencies was achieved in each case. On the basis of the optimized ground and excited state geometries, the absorption and emission properties were calculated by TD-DFT[39] at the B3LYP level. In the calculations, effective core potentials (ECP) and their associated double-ζ LANL2DZ basis set were used for the rhenium atoms,[40] while the light elements (O, N, C, and H) were described with the 6-31G(d,p) basis.[41] The contribution of every fragment in the molecules studied to the different orbitals involved in the optical transitions was calculated with the AOMix program,[42] and the graphical representation of the orbitals was made with the help of GaussView.[43]

Acknowledgements

This research was supported by the Junta de Castilla y León (Ref. VA130618). E. C. thanks the UVa for her grant. The authors in Valladolid gratefully acknowledge financial support from the Spanish MINECO, Spain (PGC2018-099470-B-I00) and and Junta de Castilla y León (VA130618), and the authors in Burgos gratefully acknowledge financial support from the Spanish MINECO, Spain (Project CTQ2015-71353-R) and Junta de Castilla y León, Consejería de Educación y Cultura y Fondo Social Europeo (Project BU051U16).

Supporting Information

The Supporting Information is available The Supporting Information is available free of charge on the ACS Publications website at DOI:

Chemical shifts of a Me_2CO-d_6 solution of **3b** after succesive additions of NaOH (aq), obtaining succesively **4b** and **5b** (Figure S1). Normalized UV/vis absorption (black) and emission (blue, λ_{ex} = 360 nm) spectra at 298 K, in deaerated solvents in optically dilute solutions. Absorption and emission (emission intensity decrease = $100 \cdot I_{non\text{-}deaerated}/I_{aerated}$) data at 298 K, in different solvents (Figure S2). Frontier Molecular Orbital Compositions (%) in the Ground State for Complexes **3a** and **4a** at the PBE1PBE Level (Tables S1 and S2). Experimental raw values observed using silver wire (as pseudoreference electrode) or AgCl/Ag (3M NaCl reference electrode) (Tables S3 and S4). Cyclic Voltammograms of *fac*-[$ReCl(CO)_3$(bipy)], **1**, **3a-d**, and **4a-d** (Figures S3 to S17). Calculated energies of the Re-pzH bond for cationic complexes and for their one-reduced-electron species (Figure S18 and Table S5).

Crystal structures of complexes 3a, 3d, and 4a. CCDC 1971286-1971288 contain the supplementary crystallographic data for this paper. These data can be obtained free of charge via www.ccdc.cam.ac.uk/data_request/cif, or by emailing data_request@ccdc.cam.ac.uk, or by contacting The Cambridge Crystallographic Data Centre, 12 Union Road, Cambridge CB2 1EZ, UK; fax: +44 1223 336033.

Author information

Corresponding Author: *(F.V.) E-mail: fernando.villafane@uva.es

ORCID: 0000-0002-3230-3802

Author Contributions: The manuscript was written through contributions of all authors. All authors have given approval to the final version of the manuscript.

Notes: The authors declare no competing financial interest.

References

[1] (a) Wrighton, M.; Morse, D. L. The nature of the lowest excited state in tricarbonylchloro-1,10-phenanthrolinerhenium(I) and related complexes. *J. Am. Chem. Soc*. **1974**, *96*, 998–1003. (b) Giordano, P.; Fredericks, S.; Wrighton, M. S.; Morse, D. Simultaneous multiple emissions from fac-XRe(CO)$_3$(3-benzoylpyridine)$_2$: n-π* intraligand and charge-transfer emission at low temperature. *J. Am. Chem. Soc.* **1978**, *100*, 2257–2259. (c) Luong, J. C.; Nadjo, L.; Wrighton, M. S. Ground and excited state electron transfer processes involving fac-tricarbonylchloro(1,10-phenanthroline)rhenium(I). Electrogenerated chemiluminescence and electron transfer quenching of the lowest excited state. *J. Am. Chem. Soc*. **1978**, *100*, 5790–5795.

[2] Some reference reviews: (a) Lees, A. J. Luminescence properties of organometallic complexes. *Chem. Rev*. **1987**, *87*, 711−743. (b) Stufkens, D. J. The remarkable properties of α-diimine rhenium tricarbonyl complexes in their metal-to-ligand chargetransfer (MLCT) excited states. *Comments Inorg. Chem*. **1992**, *13*, 359–385. (c) Schanze, K. S.; MacQueen, D. B.; Perkins, T. A.; Cabana, L. A. Studies of intramolecular electron and energy transfer using the fac-(diimine)Re^{I}(CO)$_3$ chromophore. *Coord. Chem. Rev.* **1993**, *122*, 63–89. (d) Chen, P.; Meyer, T. J. Medium effects on charge transfer in metal complexes. *Chem. Rev*. **1998**, *98*, 1439−1477. (e) Baba, A. I.; Shaw, J. R.; Simon, J. A.; Thummel, R. P.; Schmehl, R. H. The photophysical behavior of d^6 complexes having nearly isoenergetic MLCT and ligand localized excited states. *Coord. Chem. Rev*. **1998**, *171*, 43-59. (f) Stufkens, D. J.; Vlček Jr., A. Ligand-dependent excited state behaviour of Re(I) and Ru(II) carbonyl–diimine complexes. *Coord. Chem. Rev*. **1998**, *177*, 127−179. (g) Vogle, A.; Kunkely, H. Excited state properties of organometallic compounds of rhenium in high and low oxidation states. *Coord. Chem. Rev*. **2000**, *200–202*, 991–1008. (h) Yam, V. W.-W. Luminescent carbon-rich rhenium(I) complexes. *Chem. Commun*. **2001**, 789-796. (i) Striplin, D. R.; Crosby, G. A. Photophysical investigations of rhenium(I)Cl(CO)3(phenanthroline) complexes. *Coord. Chem. Rev.* **2001**, *211*, 163– 175. (j) Kirgan, R. A.; Sullivan, B. P.; Rillema, D. P. Photochemistry and photophysics of coordination compounds: rhenium. *Top. Curr. Chem.* **2007**, *281*, 45–100. (k) Coleman, A.; Brennan, C.; Vos, J. G.; Pryce, M. T. Photophysical properties and applications of Re(I) and Re(I)–Ru(II) carbonyl polypyridyl complexes. *Coord. Chem. Rev*. **2008**, *252*, 2585−2595. (l) Kumar, A.; Sun, S.-S.; Lees, A. J. Photophysics and photochemistry of organometallic rhenium diimine complexes. *Top. Organomet. Chem*. **2010**, *29*, 1−35. (m) Vlček Jr., A. Ultrafast excited-Ssate processes in Re(I) carbonyl-diimine complexes: from excitation to photochemistry. *Top. Organomet. Chem*. **2010**, *29*, 73−114. (n) Villafañe, F. Re^{I}(CO)$_3$ complexes with diimine ligands synthesized in situ. *Coord. Chem. Rev.* **2017**, *339*, 128–137.

[3] Some reference reviews: (a) Lo, K. K.-W.; Hui, W.-K.; Chung, C.-K.; Tsang, K. H.-K.; Lee, T. K.-M.; Li, C.-K.; Lau, J. S.-Y.; Ng, D. C.-M. Luminescent transition metal complex biotin conjugates. *Coord. Chem. Rev*. **2006**, *250*, 1724–1736. (b) Beck, C.; Brewer, J.; Lee, J.; McGraw, D.; DeGraff, B. A.; Demas, J. N. Localizing molecular probes: inclusion of Re(I) complexes in β-cyclodextrin. *Coord. Chem. Rev*. **2007**, *251*, 546–553. (c) Fernández-Moreira, V.; Thorp-Greenwood, F. L.; Coogan, M. P. Application of d^6 transition metal complexes in fluorescence cell imaging. *Chem. Commun*. **2010**, *46*, 186–202. (d) Lo, K. K.-W.; Louie, M.-W.; Zhang, K. Y. Design of luminescent iridium(III) and rhenium(I) polypyridine complexes as in vitro and in vivo ion, molecular and biological probes. *Coord. Chem. Rev*. **2010**, *254*, 2603−2622. (e) Lo, K. K.-W. Exploitation of luminescent organometallic rhenium(I) and iridium(III) complexes in biological studies. In "Photophysics of Organometallics", ed. A. J. Lees. *Top. Organomet. Chem*. **2010**, 73-114. (f) Balasingham, R.; Coogan, M. P.; Thorp-Greenwood, F. L. Complexes in context: attempting to control the cellular uptake and localisation of rhenium fac-tricarbonyl polypyridyl complexes. *Dalton Trans*. **2011**, *40*, 11663−11674. (g) Lo, K.-W.; Zhang, K. Y.; Li, S. P.-Y. Recent exploitation of luminescent rhenium(I) tricarbonyl polypyridine complexes as biomolecular and cellular probes. *Eur. J. Inorg. Chem.* **2011**, 3551−3568. (h) Lo, K. K.-W.; Choi, A. W.-T.; Law, W. H.-T. Applications of luminescent inorganic and organometallic transition metal complexes as biomolecular and cellular probes. *Dalton Trans*. **2012**, *41*, 6021−6047. (i) Hostachy, S.; Policar, C.; Delsuc, N. Re(I) carbonyl complexes: multimodal platforms for inorganic chemical biology *Coord. Chem. Rev*. **2017**, *351*,

172–188. (j) Lee, L. C.-C.; Leung, K.-K.; Lo, K. K.-W. Recent development of luminescent rhenium(I) tricarbonyl polypyridine complexes as cellular imaging reagents, anticancer drugs, and antibacterial agents. *Dalton Trans*. **2017**, *46*, 16357–16380. (k) Konkankit, C. C.; Marker, S. C.; Knopf, K. M.; Wilson, J. J. Anticancer activity of complexes of the third row transition metals, rhenium, osmium, and iridium. *Dalton Trans.* **2018**, *47*, 9934–9974.

[4] Some reference reviews: (a) Schanze, K. S.; MacQueen, D. B.; Perkins, T. A.; Cabana, L. A. Studies of intramolecular electron and energy transfer using the fac-(diimine)$Re^{I}(CO)_3$ chromophore. *Coord. Chem. Rev*. **1993**, *122*, 63–89. (b) Polo, A. S.; Itokazu, M. K.; Frin, K. M.; de T. Patrocínio, A. O.; Iha, N. Y. M. Light driven trans-to-cis isomerization of stilbene-like ligands in fac-$[Re(CO)_3(NN)(trans\text{-}L)]^+$ and luminescence of their photoproducts. *Coord. Chem. Rev*. **2006**, *250*, 1669−1680.

[5] Yersin, H.; Rausch, A. F.; Czerwieniec, R.; Hofbeck, T.; Fischer, T. The triplet state of organo-transition metal compounds. Triplet harvesting and singlet harvesting for efficient OLEDs. *Coord. Chem. Rev*. **2011**, *255*, 2622–2652.

[6] Some reference reviews: (a) Takeda, H.; Ishitani, O. Development of efficient photocatalytic systems for CO_2 reduction using mononuclear and multinuclear metal complexes based on mechanistic studies. *Coord. Chem. Rev*. **2010**, *254*, 346−354. (b) Qiao, J.; Liu, Y.; Hong, F.; Zhang, J. A review of catalysts for the electroreduction of carbon dioxide to produce low-carbon fuels. *Chem. Soc. Rev*. **2014**, *43*, 631-675. (c) Francke, R.; Schille, B.; Roemelt, M. Homogeneously catalyzed electroreduction of carbon dioxide–Methods, mechanisms, and catalysts. *Chem. Rev.* **2018**, *118*, 4631−4701. (d) Kuramochi, Y.; Ishitani, O.; Ishida, H. Reaction mechanisms of catalytic photochemical CO_2 reduction using Re(I) and Ru(II) complexes. *Coord. Chem. Rev*. **2018**, *373*, 333–356. (e) Jiang, C.; Nichols, A. W.; Machan, C. W. A look at periodic trends in d-block molecular electrocatalysts for CO_2 reduction. *Dalton Trans*. **2019**, *48*, 9454–9468.

[7] Zarkadoulas, A.; Koutsouri, E.; Kefalidi, C.; Mitsopoulou, C. A. Rhenium complexes in homogeneous hydrogen evolution. *Coord. Chem. Rev*. **2015**, *304–305*, 55–72.

[8] Vos, J. G. Excited-state acid-base properties of inorganic compounds. *Polyhedron* **1992**, *11*, 2285-2299.

[9] Costa, I.; Montalti, M.; Pallavicini, P.; Perotti, A.; Prodi, L.; Zaccheroni, N. Absorption and luminescence as a function of pH for carboxylic acid-functionalized Re^{I} tricarbonyls. *J. Organomet. Chem*. **2000**, *593–594*, 267–273.

[10] (a) Liu, W.; Heinze, K. Rhenium(I) and platinum(II) complexes with diimine ligands bearing acidic phenol substituents: hydrogen-bonding, acid–base chemistry and optical properties. *Dalton Trans*. **2010**, *39*, 9554–9564. (b) Chanawanno, K.; Engle, J. T.; Le, K. X.; Herrick, R. S.; Ziegler, C. J. The synthesis and pH-dependent behaviour of $Re(CO)_3$ conjugates with diimine phenolic ligands. *Dalton Trans*. **2013**, *42*, 13679–13684.

[11] Tzeng, B.-C.; Chen, B.-S.; Chen, C.-K.; Chang, Y.-P.; Tzeng, W.-C.; Lin, T.-Y.; Chou, P.-T.; Fu, Y.-J.; Chang, A. H.-H. pH-Dependent spectroscopic and luminescent properties, and metal-ion recognition studies of Re(I) complexes containing 2-(2'-pyridyl)benzimidazole and 2-(2'-pyridyl)benzimidazolate. *Inorg. Chem*. **2011**, *50*, 5379–5388.

[12] (a) Ko, C.-C.; Ng, C.-O.; Yiu, S.-M. Luminescent rhenium(I) phenanthroline complexes with a benzoxazol-2-ylidene ligand: synthesis, characterization, and photophysical study. *Organometallics* **2012**, *31*, 7074−7084. (b) Werrett, M. V.; Muzzioli, S.; Wright, P. J.; Palazzi, A.; Raiteri, P.; Zacchini, S.; Massi, M.; Stagni, S. Proton-induced reversible modulation of the luminescent output of rhenium(I), iridium(III), and ruthenium(II) tetrazolate complexes. *Inorg. Chem*. **2014**, *53*, 229−243.

[13] (a) Bronner, C.; Wenger, O. S. Proton-coupled electron transfer between 4-cyanophenol and photoexcited rhenium(I) complexes with different protonatable sites. *Inorg. Chem*. **2012**, *51*, 8275−8283. (b) Kuss-Petermann, M.; Wolf, H.; Stalke, D.; Wenger, O. S. Influence of donor−acceptor distance variation on photoinduced electron and proton transfer in rhenium(I)−phenol dyads. *J. Am. Chem. Soc*. **2012**, *134*, 12844−12854. (c) Bonn, A. G.; Neuburger, M.; Wenger, O. S. Photoinduced electron transfer in rhenium(I)−oligotriarylamine molecules. *Inorg. Chem*. **2014**, *53*, 11075−11085.

[14] Gómez-Iglesias, P.; Guyon, F.; Khatyr, A.; Ulrich, G.; Knorr, M.; Martín-Alvarez, J. M.; Miguel, D.; Villafañe, F. Luminescent rhenium(I) tricarbonyl complexes with pyrazolylamidino ligands: photophysical, electrochemical, and computational studies. *Dalton Trans*. **2015**, *44*, 17516–17528.

[15] Merillas, B.; Cuéllar, E.; Diez-Varga, A.; Asensio-Bartolomé, M.; García-Herbosa, G.; Torroba, T.; Martín-Alvarez, J. M.; Miguel, D.; Villafañe, F. Whole microwave syntheses of pyridylpyrazole and of Re and Ru luminescent pyridylpyrazole complexes. *Inorg. Chim. Acta* **2019**, *484*, 1–7.

[16] Ranjan, S.; Lin, S.-Y.; Hwang, K.-C.; Chi, Y.; Ching, W.-L.; Liu, C.-S.; Chien, T.C.-H.; Peng, S.-M.; Lee, G.-H. Realizing green phosphorescent light-emitting materials from rhenium(I) pyrazolato diimine complexes. *Inorg. Chem.* **2003**, *42*, 1248-1255.

[17] Costentin, C.; Drouet, S.; Robert, M.; Saveant, J. M. A local proton source enhances CO_2 electroreduction to CO by a molecular Fe catalyst. *Science* **2012**, *338*, 90−94.

[18] (a) Manbeck, G. F.; Muckerman, J. T.; Szalda, D. J.; Himeda, Y.; Fujita, E. Push or pull? Proton responsive ligand effects in rhenium tricarbonyl CO_2 reduction catalysts. *J. Phys. Chem. B* **2015**, *119*, 7457−7466. (b) Machan, C. W.; Yin, J.; Chabolla, S. A.; Gilson, M. K.; Kubiak, C. P. Improving the efficiency and activity of electrocatalysts for the reduction of CO_2 through supramolecular assembly with amino acid-modified ligands. *J. Am. Chem. Soc*. **2016**, *138*, 8184−8193. (c) Wilting, A.; Stolper, T.; Mata, R. A.; Siewert, I. Dinuclear rhenium complex with a proton responsive ligand as a redox catalyst for the electrochemical CO_2 reduction. *Inorg. Chem*. **2017**, *56*, 4176−4185. (d) Sinha, S.; Berdichevsky, E. K.; Warren, J. J. Electrocatalytic CO_2 reduction using rhenium(I) complexes with modified 2-(2'-pyridyl)imidazole ligands. *Inorg. Chim. Acta* **2017**, *460*, 63–68. (e) Sung, S.; Kumar, D.; Gil-Sepulcre, M.; Nippe, M. Electrocatalytic CO_2 reduction by imidazolium-functionalized molecular catalysts. *J. Am. Chem. Soc*. **2017**, *139*, 13993−13996. (f) Rotundo, L.; Garino, C.; Priola, E.; Sassone, D.; Rao, H.; Ma, B.; Robert, M.; Fiedler, J.; Gobetto, R.; Nervi, C. Electrochemical and photochemical reduction of CO_2 catalyzed by Re(I) complexes carrying local proton sources. *Organometallics* **2019**, *38*, 1351−1360. (g) Das, T.; Rajak, K. K. Experimental and theoretical investigation of a metalloreceptor bearing a $[Re(CO)_3]^+$ core incorporating a multifunctional ligand: selective reactivity towards Zn^{2+} and CN^- ions. *Dalton Trans.* **2019**, *48*, 6879–6891 .

[19] Arroyo, M.; Gómez-Iglesias, P.; Antón, N.; García-Rodríguez, R.; Alegria, E. C. B. A.; Pombeiro, A. J. L.; Miguel, D.; Villafañe, F. Homo- and heteropolymetallic 3-(2-pyridyl)pyrazolate manganese and rhenium complexes. *Dalton Trans*. **2014**, *43*, 4009–4020.

[20] See for example: (a) Lytwak, L. A.; Stanley, J. M.; Mejía, M. L.; Holliday, B. J. Synthesis, characterization, and photophysical properties of a thiophene-functionalized bis(pyrazolyl) pyridine (BPP) tricarbonyl rhenium(I) complex. *Dalton Trans*. **2010**, *39*, 7692–7699. (b) Wei, Q.-H.; Xiao, F.-N.; Han, L.-J.; Zeng, S.-L.; Duan, Y.-N.; Chen, G.-N. Synthesis, structure, photophysical and electrochemiluminescence properties of Re(I) tricarbonyl complexes incorporating pyrazolyl–pyridyl-based ligands. *Dalton Trans*. **2011**, *40*, 5078–5085. (c) Sangilipandi, S.; Nagarajaprakash, R.; Sutradhar, D.; Kaminsky, W.; Chandra, A. K.; Rao, K. M. Synthesis, molecular structural studies and DFT calculations of tricarbonylrhenium(I) metal complexes containing nitrogen based N∩N donor polypyridyl ligands. *Inorg. Chim. Acta* **2015**, *437*, 177–187. (d) Saad, S. T.; Metherell, A. J.; Baggaley, E.; Ward, M. D. Synthesis and photophysical properties of Ir(III)/Re(I) dyads: control of Ir→Re photoinduced energy transfer. *Dalton Trans*. **2016**, *45*, 11568–11579. (e) Sangilipandi, S.; Sutradhar, D.; Bhattacharjee, K.; Kaminsky, W.; Joshi, S. R.; Chandra, K.; Rao, K. M. Synthesis, structure, antibacterial studies and DFT calculations of arene ruthenium, Cp⁄Rh, Cp⁄Ir and tricarbonylrhenium metal complexes containing 2-chloro-3-(3-(2-pyridyl)pyrazolyl)quinoxaline ligand. *Inorg. Chim. Acta* **2016**, *441*, 95–108.

[21] (a) Jeffrey, G.A. *An Introduction to Hydrogen Bonding*, Oxford University Press, New York, 1997. Ch. 2. (b) Steiner, T. The Hydrogen Bond in the Solid State. *Angew. Chem., Int. Ed*. **2002**, *41*, 48–76.

[22] (a) Catalán, J.; Claramunt, R. M.; Elguero, J.; Laynez, J.; Menéndez, M.; Anvia, F.; Quian, J. H.; Taagepera, M.; Taft, R. W. Basicity and Acidity of Azoles: The annelation effect in azoles. *J. Am. Chem. Soc*. **1988**, *110*, 4105−4111. (b) Elguero, J.; Yranzo, G. I.; Laynez, J.; Jiménez, P.; Menéndez, M.; Catalán, J.; de Paz, J. L. G.; Anvia, F.; Taft, R. W. Effect of the replacement of a methyl by a trifluoromethyl group on the acid-base properties of pyrazoles. *J. Org. Chem*. **1991**, *56*, 3942−3947.

[23] Wright, P. J.; Affleck, M. G.; Muzzioli, S.; Skelton, B. W.; Raiteri, P.; Silvester, D. S.; Stagni, S.; Massi, M. Ligand-induced structural, photophysical, and electrochemical variations in tricarbonyl rhenium(I) tetrazolato complexes. *Organometallics* **2013**, *32*, 3728−3737.

[24] Werrett, M. V.; Chartrand, D.; Gale, J. D.; Hanan, G. S.; MacLellan, J. G.; Massi, M.; Muzzioli, S.; Raiteri, P.; Skelton, B. W.; Silberstein, M.; Stagni, S. Synthesis, structural, and photophysical investigation of diimine triscarbonyl Re(I) tetrazolato complexes. *Inorg. Chem*. **2011**, *50*, 1229–1241.

[25] (a) Shavaleev, N. M.; Bell, Z. R.; Easun, T. L.; Rutkaite, R.; Swanson, L.; Ward, M. D. Complexes of substituted derivatives of 2-(2-pyridyl)benzimidazole with Re(I), Ru(II) and Pt(II): structures, redox and luminescence properties. *Dalton Trans*. **2004**, 3678–3688. (b) Obata, M.; Kitamura, A.; Mori, A.; Kameyama, C.; Czaplewska, J. A.; Tanaka, R.; Kinoshita, I.; Kusumoto, T.; Hashimoto, H.; Harada, M.; Mikata, Y.; Funabiki, T.; Yano, S. Syntheses, structural characterization and photophysical properties of 4-(2-pyridyl)-1,2,3-triazole rhenium(I) complexes. *Dalton Trans*. **2008**, 3292–3300. (c) Wolff, M.; Munoz, L.; François, A.; Carrayon, C.; Seridi, A.; Saffon, N.; Picard, C.; Machura, B.; Benoist, E. Tricarbonylrhenium complexes from 2-pyridyl-1,2,3-triazole ligands bearing a 4-substituted phenyl arm: a combined experimental and theoretical study. *Dalton Trans*. **2013**, *42*, 7019–7031. (d) Klemens, T.; Czerwińska, K.; Szlapa-Kula, A.; Kula, S.; Świtlicka, A.; Kotowicz, S.; Siwy, M.; Bednarczyk, K.; Krompiec, S.; Smolarek, K.; Maćkowski, S.; Danikiewicz, W.; Schab-Balcerzak, E.; Machura, B. Synthesis, spectroscopic, electrochemical and computational studies of rhenium(I) tricarbonyl complexes based on bidentate-coordinated 2,6-di(thiazol-2-yl)pyridine derivatives. *Dalton Trans*. **2017**, *46*, 9605–9620.

[26] Cattaneo, M.; Fagalde, F.; Katz, N. E. Proton-induced luminescence of mono- and dinuclear rhenium(I) tricarbonyl complexes containing 4-pyridinealdazine. *Inorg. Chem*. **2006**, *45*, 6884-6891.

[27] Gritzner, G.; Kuta, J. Recommendations on reporting electrode potentials in nonaqueous solvents. *Pure Appl. Chem*. **1984**, *56*, 461–466.
[28] Bullock, J. P.; Carter, E.; Johnson, R.; Kennedy, A. T.; Key, S. E.; Kraft, B. J.; Saxon, D.; Underwood, P. Reactivity of electrochemically generated rhenium (II) tricarbonyl α-diimine complexes: a reinvestigation of the oxidation of luminescent $Re(CO)_3$(α-diimine)Cl and related compounds. *Inorg. Chem*. **2008**, *47*, 7880–7887.
[29] (a) Zeng, Q.; Messaoudani, M.; Vlček, A.; Hartl, F. Electrochemical reductive deprotonation of an imidazole ligand in a bipyridine tricarbonyl rhenium(I) complex. *Eur. J. Inorg. Chem*. **2012**, 471–474. (b) Zeng, Q.; Messaoudani, M.; Vlček, A.; Hartl, F. Temperature-dependent reduction pathways of complexes fac-$[Re(CO)_3$(N-R-imidazole)(1,10-phenanthroline)$]^+$ (R = H, CH_3). *Electrochim. Acta* **2013**, *110*, 702–708.
[30] Hawecker, J.; Lehn, J.-M.; Ziessel, R. Electrocatalytic reduction of carbon dioxide mediated by Re(bipy)$(CO)_3$Cl (bipy = 2,2'-bipyridine). *J. Chem. Soc., Chem. Commun*. **1984**, 328-330.
[31] Klein, A.; Vogler, C.; Kaim, W. The δ in 18 + δ electron complexes: importance of the metal/ligand interface for the substitutional reactivity of "Re(0)" complexes (α-diimine$^-$)$Re^I(CO)_3$(X). *Organometallics* **1996**, *15*, 236–244.
[32] Anderson, C. B.; Elliott, A. B. S.; McAdam, C. J.; Gordon, K. C.; Crowley, J. D. fac-$Re(CO)_3$Cl complexes of [2-(4-R-1H-1,2,3-Triazol-1-yl)methyl]pyridine inverse "click" ligands: a systematic synthetic, spectroscopic, and computational study. *Organometallics* **2013**, *32*, 788–797.
[33] Gómez-Iglesias, P.; Guyon, F.; Khatyr, A.; Ulrich, G.; Knorr, M.; Martín-Alvarez, J. M.; Miguel, D.; Villafañe, F. Luminescent rhenium(I) tricarbonyl complexes with pyrazolylamidino ligands: photophysical, electrochemical, and computational studies. *Dalton Trans*. **2015**, *44*, 17516–17528.
[34] Perrin D. D.; Armarego, W. L. F. *Purification of Laboratory Chemicals*, Pergamon Press, Oxford, 3rd edn, 1988.
[35] ^{1}H NMR (CD_3NO_2): δ: 7.13 (d, J = 2.8 Hz, H^4, 1 H), 7.54 (dd, J = 4.8 y 2.8 Hz, $H^{5'}$, 1 H), 7.96 (d, J = 2.8 Hz, H^5, 1 H), 8.13 (m, $H^{4'}$ and $H^{3'}$, 2 H), 9.0 (d, J = 5.2 Hz, $H^{6'}$, 1 H), 12.90 (br s, N*H*, 1 H). In other solvents the ^{1}H NMR spectra display a mixture of compounds as a result of the substitution of the triflate ligand by residual THF and/or the deuterated solvent. IR (THF, cm^{-1}): 2035 s, 1933 s, 1910 s, assigned to *fac*-$[Re(CO)_3$(pypzH)(thf)]OTf.
[36] (a) Fujita, E.; Creutz, C.; Sutin, N.; Szalda, D. J. Carbon dioxide activation by cobalt(I) macrocycles: factors affecting carbon dioxide and carbon monoxide binding. *J. Am. Chem. Soc*. **1991**, *113*, 343–353. (b) Gennaro, A.; Isse, A. A.; Vianello, E. Solubility and electrochemical determination of carbon dioxide in some dipolar aprotic solvents. *J. Electroanal. Chem*. **1990**, *289*, 203–215.
[37] Gaussian 16, Revision A.03, Frisch, M. J.; Trucks, G. W.; Schlegel, H. B.; Scuseria, G. E.; Robb, M. A.; Cheeseman, J. R.; Scalmani, G.; Barone, V.; Petersson, G. A.; Nakatsuji, H.; Li, X.; Caricato, M.; Marenich, A. V.; Bloino, J.; Janesko, B. G.; Gomperts, R.; Mennucci, B.; Hratchian, H. P.; Ortiz, J. V.; Izmaylov, A. F.; Sonnenberg, J. L.; Williams-Young, D.; Ding, F.; Lipparini, F.; Egidi, F.; Goings, J.; Peng, B.; Petrone, A.; Henderson, T.; Ranasinghe, D.; Zakrzewski, V. G.; Gao, J.; Rega, N.; Zheng, G.; Liang, W.; Hada, M.; Ehara, M.; Toyota, K.; Fukuda, R.; Hasegawa, J.; Ishida, M.; Nakajima, T.; Honda, Y.; Kitao, O.; Nakai, H.; Vreven, T.; Throssell, K.; Montgomery, Jr., J. A.; Peralta, J. E.; Ogliaro, F.; Bearpark, M. J.; Heyd, J. J.; Brothers, E. N.; Kudin, K. N.; Staroverov, V. N.; Keith, T. A.; Kobayashi, R.; Normand, J.; Raghavachari, K.; Rendell, A. P.; Burant, J. C.; Iyengar, S. S.; Tomasi, J.; Cossi, M.; Millam, J. M.; Klene, M.; Adamo, C.; Cammi, R.; Ochterski, J. W.; Martin, R. L.; Morokuma, K.; Farkas, O.; Foresman, J. B.; Fox, D. J. Gaussian, Inc., Wallingford CT, 2016.
[38] (a) Becke, A. D. Density-functional thermochemistry. III. The role of exact exchange. *J. Chem. Phys.* **1993**, *98*, 5648-5652. (b) Lee, C.; Yang, W.; Parr, R. G. Development of the Colle-Salvetti correlation-energy formula into a functional of the electron density. *Phys. Rev. B*, **1988**, *37*, 785. (c) Hay, P. J.; Wadt, W. R. Ab initio effective core potentials formolecular calculations. Potentials for K toAu including the outermost core orbitals. *J. Chem. Phys.*, 1985, **82**, 299-310.
[39] (a) Helgaker, T.; Jorgensen, P. An electronic Hamiltonian for originindependent calculations of magneticproperties. *J. Chem. Phys.* **1991**, *95*, 2595-2601. (b) Bak, K. L.; Jorgensen, P.; Helgaker, T.; Rund, K.; Jenson, H. J. A. Gauge-origin independentmulticonfigurational self-consistent-fieldtheory for vibrational circular dichroism. *J. Chem. Phys.* **1993**, *98*, 8873-8887. (c) Autschbach, A.; Ziegler, T.; Gisbergen, S. J. A.; Baerends, E. J. Chiroptical properties from time-dependent density functional theory. I. Circular dichroism spectra of organic molecules. *J. Chem. Phys.* **2002**, *116*, 6930-6940.
[40] (a) Hay, P. J.; Wadt, W. R. Ab initio effective core potentials for molecular calculations. Potentials for the transition metal atoms Sc to Hg. *J. Chem. Phys.* ***1985***, *82*, 270-283. (b) Hay, P. J.; Wadt, W. R. Ab initio effective core potentials for molecular calculations. Potentials for K to Au including the outermost core orbitals. *J. Chem. Phys.* **1985**, *82*, 299-310.
[41] (a) Gabrielsson, A.; Matousek, P.; Towrie, M.; Hartl, F.; Zalis, S.; Vlček Jr., A. Excited states of nitro-polypyridine metal complexes and their ultrafast decay. Time-resolved IR absorption, spectroelectrochemistry,

and TD-DFT calculations of fac-[Re(Cl)$(CO)_3$(5-Nitro-1,10-phenanthroline)]. *J. Phys. Chem. A* **2005**, *109*, 6147-6153. (b) Dattelbaum, D. M.; Omberg, K. M.; Hay, P. J.; Gebhart, N. L.; Martin, R. L.; Schoonover, J. R.; Meyer, T. J. Defining electronic excited states using time-resolved infrared spectroscopy and density functional theory calculations. *J. Phys. Chem. A* **2004**, *108*, 3527-3536. (c) Dattelbaum, D. M.; Martin, R. L.; Schoonover, J. R.; Meyer, T. J. Molecular and electronic structure in the metal-to-ligand charge transfer excited states of fac-[Re(4,4'-X_2bpy)$(CO)_3$(4-Etpy)]$^{+}$* (X = CH_3, H, CO_2Et). Application of density functional theory and time-resolved infrared spectroscopy. *J. Phys. Chem. A* **2004**, *108*, 3518-3526. (d) Lundin, N. J.; Walsh, P. J.; Howell, S. L.; McGarvey, J. J. ; Blackman, A. G.; Gordon, K. C. Complexes of functionalized dipyrido[3,2-a:2',3'-c]-phenazine: a synthetic, spectroscopic, structural, and density functional theory study. *Inorg. Chem.* **2005**, *44*, 3551-3560.

[42] (a) Gorelsky, S. I. *AOMix: Program for Molecular Orbital Analysis*, http://www.sg-chem.net/, University of Ottawa, version 6.5, 2011. (b) Gorelsky, S. I.; Lever, A. B. P. Electronic structure and spectra of ruthenium diimine complexes by density functional theory and INDO/S. Comparison of the two methods. *J. Organomet. Chem.* **2001**, *635*, 187-196.

[43] GaussView, Version 5, Dennington, R.; Keith, T.; Millam, J. *Semichem Inc.*, Shawnee Mission KS, 2009.

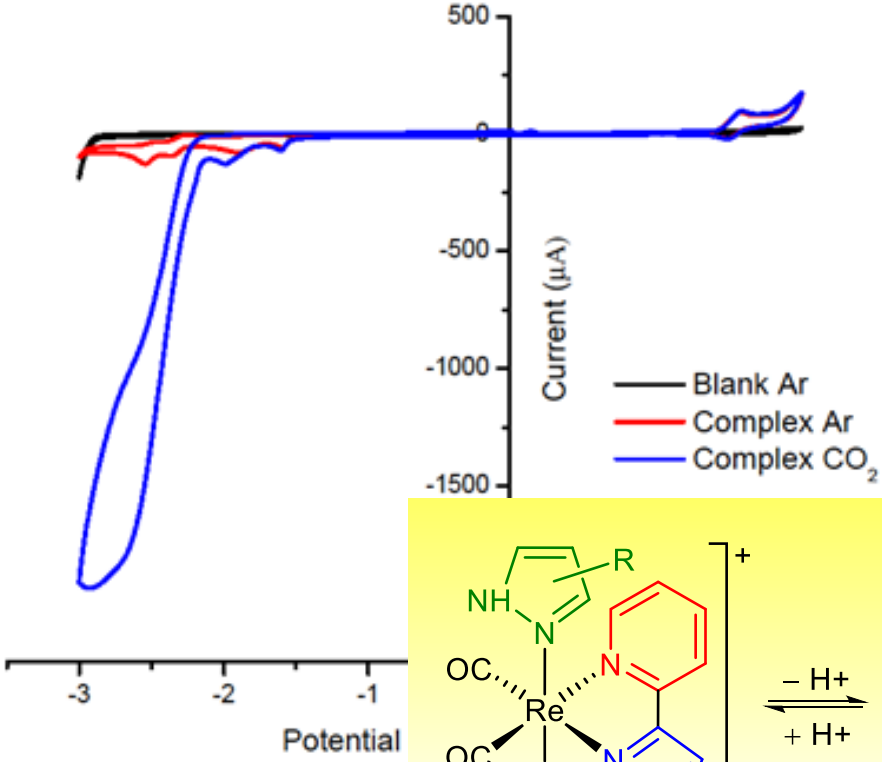
500
0
-500
-1000
-1500
Current (μA)
-3
-2
-1
Potential
Blank Ar
Complex Ar
Complex CO2

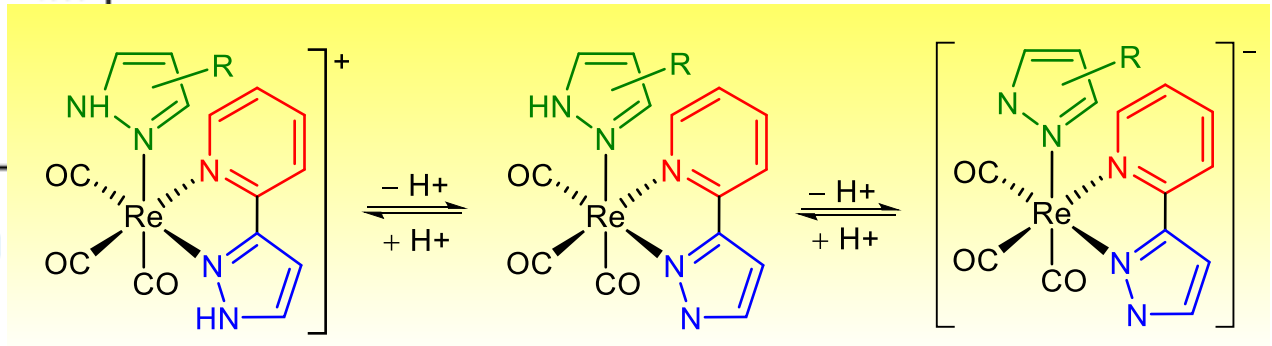
R
NH
N
OC
Re
OC
CO
N
N
HN
+
– H+
+ H+
HN
N
OC
Re
OC
CO
N
N
– H+
+ H+
N
N
OC
Re
OC
CO
N
N
–

Luminescent Rhenium(I)tricarbonyl complexes containing different pyrazoles and their Successive Deprotonation Products: CO_2 Reduction Electrocatalysts

Beatriz Merillas,[a] Elena Cuéllar,[a] Alberto Diez-Varga,[b] Tomás Torroba,[b] Gabriel García-Herbosa,[b] Jose M. Martín-Alvarez,[a] Daniel Miguel,[a] and Fernando Villafañe[a]

[a] *GIR MIOMeT-IU Cinquima-Química Inorgánica, Facultad de Ciencias, Campus Miguel Delibes, Universidad de Valladolid, 47011 Valladolid, Spain. E-mail: fernando.villafane@uva.es*

[b] *Departamento de Química, Facultad de Ciencias, Universidad de Burgos, 09001 Burgos, Spain.*

TABLE OF CONTENTS

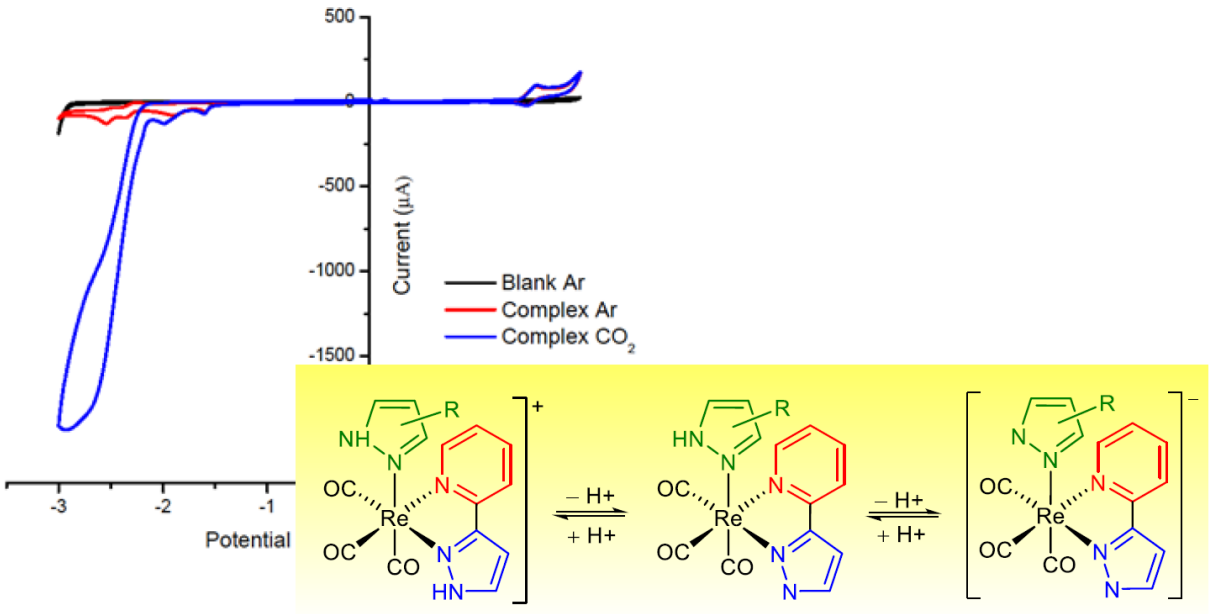

A family of cationic complexes, containing pypzH and different pyrazoles (pzH, dmpzH, indzH and pypzH) coordinated to the *fac*-[ReBr(CO)$_3$] fragment, allow successive deprotonations in order to obtain neutral and anionic compounds with similar ligands, but different electronic and steric properties. They exhibit phosphorescent behavior consistent with a prevalently ^{3}MLCT excited state. Their electrochemical behavior both in Ar atmosphere and under CO_2 is described. The latter is consistent with CO_2 electrocatalyzed reduction.